We are very grateful to the evaluations from the reviewers, which have allowed us to clarify and improve the manuscript. Below we addressed the reviewer comments, with the reviewer comments in black and our response in blue.

Before we provide the detailed point by point reply, we provide an overview of the main changes and improvements:

1. **We added some detailed descriptions of the model and model output in Section 2 Data and Method.**

2. **We added four sensitivity tests related to reaction rate during HOMs formation and their description in Section 2.4.**

3. **We added a new Section to discuss the impact of uncertainties from HOMs chemistry on aerosol and CCN number.**

4. **In the last Section (Summary), we added more discussion on the limitations and uncertainties associated with our current results.**

Reply for the referee comment#1

General comments: This paper details work on implementing a HOM chemistry scheme into a large-scale model and comparing the results with an updated inorganic-only nucleation scheme. The inclusion of organic nucleation and growth at small particle sizes due to HOM formation leads to better agreement overall with measurements of high altitude CCN and frequency of NPF events globally. This work provides an interesting look into incorporating HOM chemistry into global models. The results seem reasonable and fit within the scope of ACP. My main concern stems from a lack sensitivity studies surrounding many of the uncertainties in the mechanism as well as a lack of discussion of the limitations of the mechanism. Given HOM chemistry is an active area of research, it makes these results incredibly significant to the community, but also means communicating clearly the limitations of the work given the present understanding of HOM chemistry is all the more important. Overall, I think this paper presents an important contribution to the field and I would support publication if the following comments are addressed.

General Response: We greatly appreciate the referee for their time and efforts devoted to the review of our submission. We realize that most of the comments are due to the missing sensitivity studies of exploring possible uncertainties from HOMs chemistry. We will present these details in the following responses.

Specific comments and responses:

Major Comment#1: The sensitivity studies done in this work seem informative, but more should be done on the other unknown parameters related to HOM formation such as the autoxidation rate coefficient, the temperature-dependence of this rate coefficient, and the dimerization rate coefficients.

Response: We agree with the reviewer the HOMs concentrations are affected by many parameters. We have added a discussion section (**Section 5**) about the potential uncertainties in autoxidation rate, autoxidation temperature dependence, and dimerization reaction rate with five extra sensitivity tests. The discussion of the original sensitivity tests related to HOMs chemistry (i.e. "Slow_NO" and "Low_Br") were also moved to this new Section (**Section 5**) as all of them are related to uncertainties from organic chemistry. Details of five additional sensitivity tests are listed in two new tables in the **Supplementary Information** (Table S7 and S8)

Table 2 in **Section 2.4 (Sensitivity experiments)** was also modified as follows (added five sets of sensitivity experiments, labeled "High_temp", "Low_temp", "Fast_auto", "Slow_auto" and "Slow_accr" in the last five lines):

Table 1. Configurations of CESM2.1.0 Experiments

Test Name	Updated inorganic nucleation	HOMs chemistry	Organic Nucleation	Organic Growth	Other Changes
Default	×	×	×	×	/
Inorg	✓	✓	×	×	/
Inorg_Org	✓	✓	✓	✓	/
Only_NR	✓	✓	✓	×	/
Only_GR	✓	✓	×	✓	/
Low_Br	✓	✓	✓	✓	Lower branch ratio of the first-generation product (MT-RO_2) from MT + O_3 and MT + OH, which could be further auto-oxidized
Slow_NO	✓	✓	✓	✓	Rate of MT-HOM-RO_2 (second-generation autoxidation product) + NO generating HOMs, multiplied by 0.2
High_temp	✓	✓	✓	✓	Autoxidation rate with high temperature dependence (Roldin et al., 2019) (Table S7)
Low_temp	✓	✓	✓	✓	Autoxidation rate with low temperature dependence (Weber et al., 2020) (Table S7)
Fast_auto	✓	✓	✓	✓	Autoxidation rate multiplied by 10
Slow_auto	✓	✓	✓	✓	Autoxidation rate multiplied by 0.1

Slow_accr	✓	✓	✓	✓	Using slower self-/cross reaction rate derived from Weber et al. (2020) and Berndt et al. (2018) (Table S8)

The description of these sensitivity tests (Table 2) in **Section 2.4** were modified as (The underlined content is newly added or modified):

"We also conducted five sensitivity simulations to examine uncertainties in concentrations of HOMs (Table 2): sensitivity to the branching ratio from the first generation of monoterpene (MT) reactions with O_3/OH that can be auto-oxidized (Low_Br), sensitivity to the rate of termination reaction involving NO (Slow_NO), sensitivity to the autoxidation temperature dependence (High_temp and Low_temp), sensitivity to the autoxidation rate (Fast_auto and Slow_auto) and sensitivity to the self-/cross-reaction rate (Slow_accr) (Table 2). In Inorg_Org, the branching ratios for the MT-derived peroxyl radicals (MT-bRO_2) which could be further auto-oxidized are set at 80% for MT+O_3 and 97% for MT+OH reactions, corresponding to the high values reported in Xu et al. (2022). In the Low_Br simulation (Table 2), the branching ratio for MT-RO_2 is set as 25% for MT + O_3 and 92% and MT + OH. Both the high and low branching ratios fall within the range of previous studies (Lee et al., 2023; Pye et al., 2019; Weber et al., 2020; Xu et al., 2018; Jokinen et al., 2015; Roldin et al., 2019). In Slow_NO, the reaction rate of MT-HOM-RO_2+NO (MT-HOM-RO_2, the second-generation product of autoxidation (Text S1) is set as one-fifth of that in Inorg_Org, given that the simulated NO concentration is fourfold higher than the measured values in the boreal forest in Finland and in the southeast USA (Fig. S3 and S2 in Liu et al. (2024)). In High_temp and Low_temp, the temperature dependence of autoxidation rate are set to lower and upper limits (i.e. representing possible higher and lower bound of activation energy, Table S7) based on chamber experiments (Roldin et al., 2019; Weber et al., 2020). In Fast_auto and Slow_auto, the autoxidation reaction rates are multiplied by 10 and 0.1 respectively. In Slow_accr, the rate of self-/cross- reactions are set as the lower value (Table S8) based on chamber experiments (Weber et al., 2020; Berndt et al., 2018)."

We have added a new section "**5 Uncertainties from HOMs chemistry**". The content is as follows:

"This section aims to test the effect of using different autoxidation and self-/cross reaction rates as well as branching ratios during HOMs and ACC formation on the 1 nm nucleation rate, sub-20nm growth rate, total aerosol number concentration and CCN number concentration.

The change of the autoxidation rate (Fast_auto and Slow_auto) affects both the nucleation and growth rates, particularly within the HOMs source regions. A higher autoxidation rate leads to higher intermediate radical concentrations and thus more HOMs. Multiplying the autoxidation rate by 10 (Fast_auto) leads to a 6% increase in the nucleation rate and a 3% increase in the sub-20nm growth

rate on a global average (Fig. S11). The largest increases occur in regions such as the Amazon, Australia and boreal forests (>10%) where HOMs is most abundant. In these regions, the aerosol number concentration increased by more than 30% compared to the baseline Inorg_Org. Conversely, in Slow_auto, the nucleation and growth rates decline by 17% and 5%, respectively, resulting in a 15% reduction in aerosol number and a 6% reduction in CCN number globally. In the Amazon and boreal forests, the reductions exceed 20% (Table 5).

Adjusting the autoxidation temperature dependence to upper and lower limits (High_temp and Low_temp) causes changes in HOMs concentration (Fig. S10). However, its impact on nucleation (-7% and -4% in High_temp and Low_temp), growth rate (-4% and ~0% in High_temp and Low_temp), aerosol (-12% and 3% in High_temp and Low_temp) and CCN (-4% and ~0% in High_temp and Low_temp) number concentrations are small (Fig. S11 and S12). This is because most of these changes occur over ocean, where H_2SO_4 has low concentrations. Consequently, the rate of heteromolecular nucleation of sulfuric acid and organics (HET), which is the greatest contributor to the organic-involving nucleation rate, does not show significant change in both experiments.

A lower dimerization reaction rate leads to decreased concentrations of accretion products (ACC), with a 71% decrease in the Slow_accr. Lower consumption of MT-derived peroxyl radicals (MT-RO_2) during self-/cross- reaction means more of them can participate in autoxidation. This explains the higher HOMs concentration over source regions in Slow_accr compared to Inorg_Org (Fig. S10). However, the impact of slowing down the dimerization rate on aerosol and CCN number concentrations is negligible, remaining within 1% on a global average. In the Slow_accr experiment, the nucleation rate in the Amazon, where the concentration of ACC is highest, decreases by more than 50%, subsequently leading to a reduction of more than 20% in aerosol and CCN numbers (Table 5). This implies that both aerosol and CCN number concentration in the Amazon basin are sensitive to the ACC concentration.

The change of HOMs and ACC concentration in Slow_NO is almost negligible (-6% and 5%) hence its impact on aerosol and CCN number can be ignored (~0%). When the rate of NO termination is reduced, less MT-HOM-RO_2 was consumed when generating HOMs, and thus more MT-HOM-RO_2 participates in self-/cross-reactions. This explains the higher concentration of ACC and lower concentration of HOMs in the Slow_NO compared to Inorg_Org. In contrast, in the Low_Br, there is a significant decrease in HOMs concentration (-51%) (Fig. S10) since the mass yield of MT-bRO_2 is decreased, which subsequently leads to a 17% reduction in the nucleation rate (Fig. S11). Combining with approximately a 5% reduction in the growth rate of sub-20nm particles, the concentrations of aerosol and CCN decrease by -12% and -5% respectively (Table 5). In regions most sensitive to

biogenic HOMs chemistry, such as the Amazon, Australia, and boreal forests, the reduction in particle concentrations exceeds 20%."

Also, we added Table 5 (see below) in the main text of **Section 5** to present the values more directly:

Table 2. Relative differences (Units: unitless) of vertically-integrated HOMs concentrations (HOMs), accretion products concentrations (ACC), nucleation (NR), growth rate (GR), aerosol number (Aerosol), and CCN number (CCN) in July 2013 between Inorg_Org and other sensitivity tests. Values in the table are global mean values. Model experiments are described in Table 2.

	HOMs	ACC	NR	GR	Aerosol	CCN
Slow_NO	-6%	5%	-2%	~0	~0	~0
Low_br	-51%	-12%	-17%	-5%	-12%	-5%
High_temp	-42%	-6%	-7%	-4%	-12%	-4%
Low_temp	9%	~0	-4%	~0	3%	~0
Fast_auto	75%	8%	6%	3%	18%	4%
Slow_auto	-57%	-5%	-17%	-5%	-15%	-6%
Slow_accr	66%	-71%	-4%	~0	-2%	-1%

Table S7 and S8 and Figure S10, S11 and S12 are shown as follow:

Table S7. Description of sensitivity test for the autoxidation rate with different temperature dependency (Roldin et al., 2019; Weber et al., 2020).

Test Name	Reaction rate for generating	
	$MT\text{-}cRO_2$ (first-generation autoxidation products)	$MT\text{-}HOM\text{-}RO_2$ (multi-generation autoxidation products)
Low_temp	1.009E9*exp(-6000/T)	9.500E8*exp(-6000/T)
High_temp	7.768E17*exp(-12077/T)	7.311E17*exp(-12077/T)
Inorg_Org	9.800E12*exp(-8836/T)	9.800E12*exp(-8836/T)

Table S8. Description of sensitivity test for the different self-/cross- reaction rate (Weber et al., 2020; Berndt et al., 2018).

Test Name	Reaction rate for generating	
	C15	C20
Slow_accr	1.800e-12	0.400e-11
Inorg_Org	2.000~4.000e-11	4.000~26.000e-11

We are grateful to the referee for highlighting these important uncertainties of HOMs and ACC chemistry so we have included the following discussion at the **Summary**:

"We also test the sensitivity of aerosol number concentrations to uncertainties from HOMs chemistry. Results show that including organic NPF processes in our model is more important than tuning these aspects of the parametrizations during HOMs formation. Compared to the baseline Inorg_Org model, decreasing the branching ratio of the first-generation product from Monoterpene+O_3/OH, which could further undergo autoxidation (Low_Br), leads to only a 12% reduction in global average vertically-integrated aerosol number concentrations. Slowing down NO-involved chemical reactions due to NO concentration overestimation at two stations (Slow_NO) has very little effect on the global average aerosol number concentration (within ~1%) (Fig. 10). When altering the temperature dependence of autoxidation rate into higher or lower value (High_temp and Low_temp), HOMs concentrations change a lot (-42% and 9% respectively) but aerosol number concentrations only change a small amount (-12% and 3%). Factor of 10 changes of autoxidation rate (multiplying the autoxidation rate by 10 in Fast_auto and 0.1 in Slow_auto) results in a relatively significant changes in the simulated aerosol number concentration (18% and -15% in global mean). When adjusting the dimerization rate coefficient of ACC formation to lower value (Slow_accr), the aerosol number change is negligible (within 2% on global average). Except for Amazon, the aerosol number concentrations are highly sensitive to ACC concentration and decrease by about more than 20%."

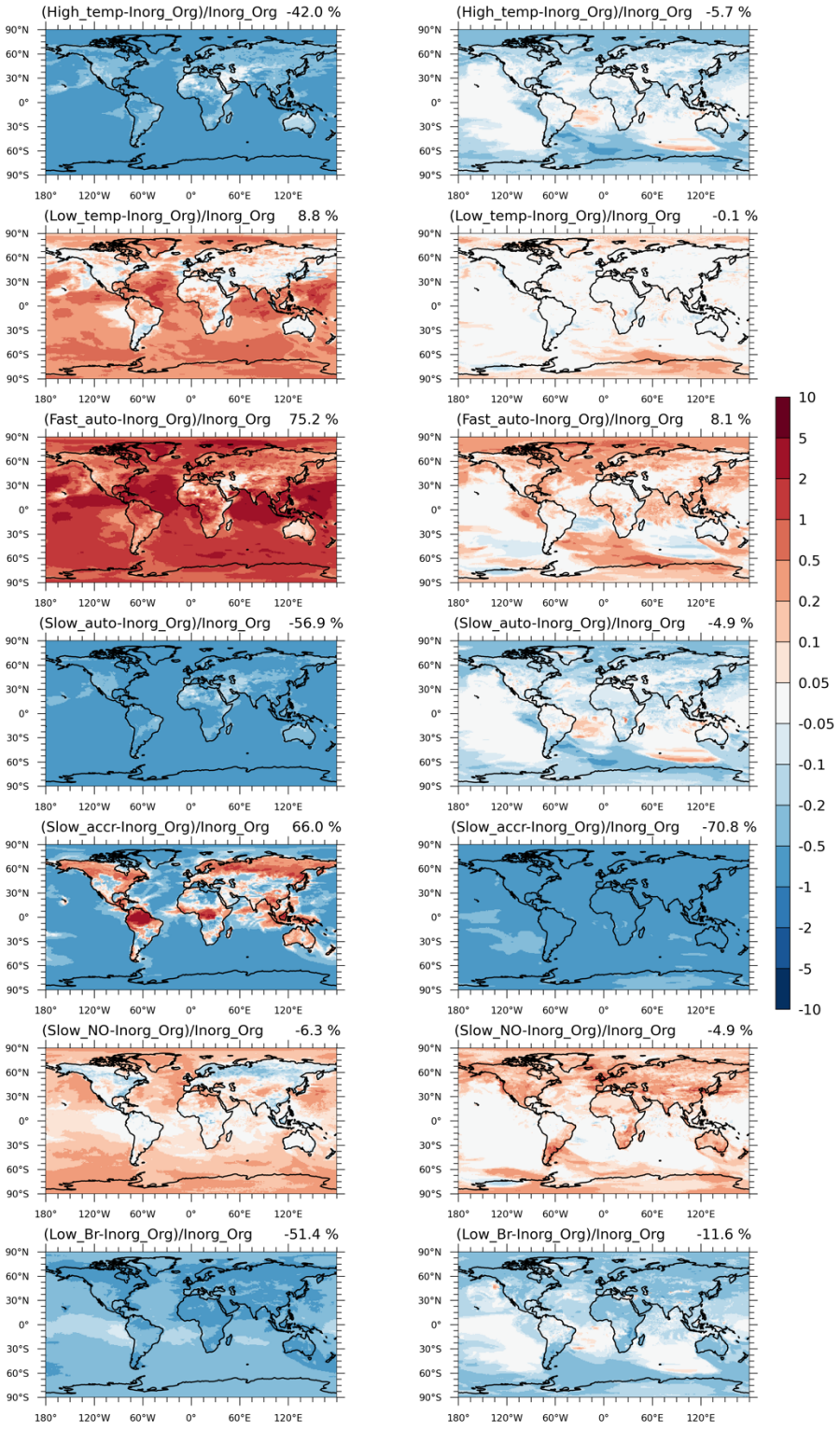

Figure S10. Relative differences (Units: unitless) of vertically-integrated HOMs (left column) and accretion products (right column) in July 2013 between Inorg_Org and other sensitivity tests. Global mean values are shown on the top right of each figure. Model experiments are described in Table 2.

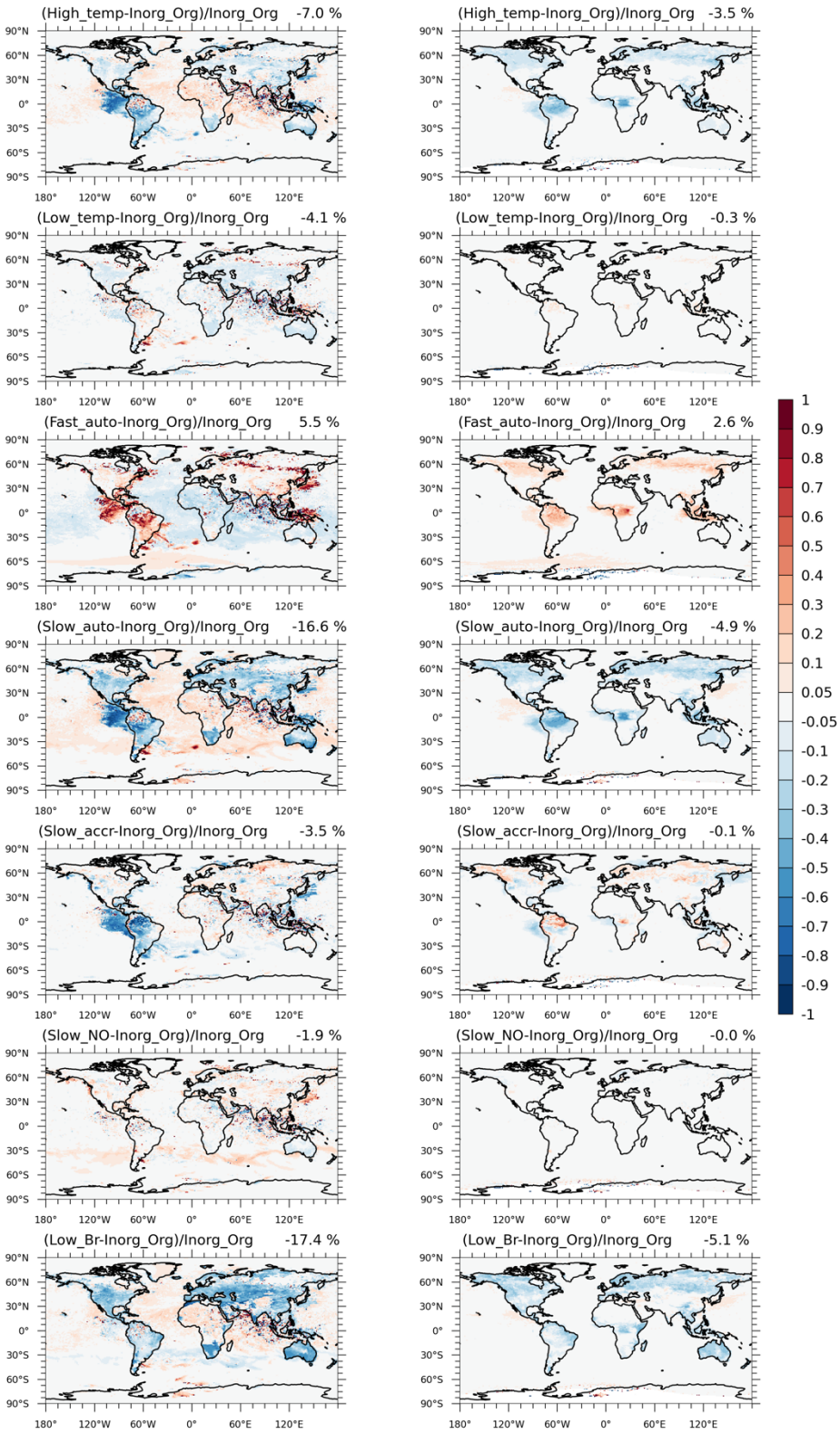

Figure S11. Relative differences (Units: unitless) of vertically-integrated nucleation (left column) and growth rate (right column) in July 2013 between Inorg_Org and other sensitivity tests. Global mean values are shown on the top right of each figure. Model experiments are described in Table 2.

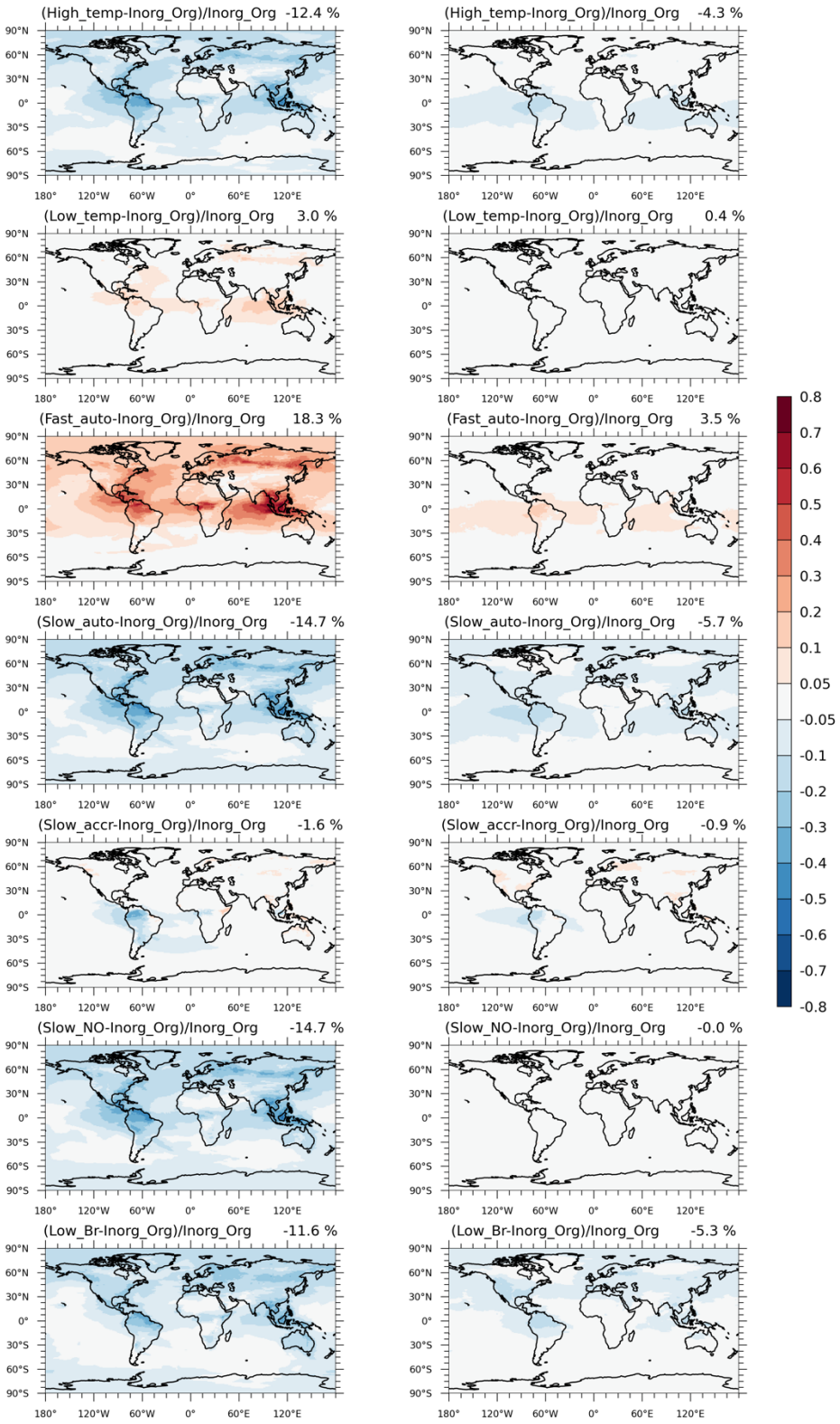

Figure S12. Relative differences (Units: unitless) of vertically-integrated aerosol (a, c, e, g, I and k) and CCN number concentration (b, d, f, h, j and l) in July 2013 between Inorg_Org and other sensitivity tests. Global mean values are shown on the top right of each figure. Model experiments are described in Table 2.

Reference

Berndt, T., Mentler, B., Scholz, W., Fischer, L., Herrmann, H., Kulmala, M., and Hansel, A.: Accretion Product Formation from Ozonolysis and OH Radical Reaction of α-Pinene: Mechanistic Insight and the Influence of Isoprene and Ethylene, Environ. Sci. Technol., 52, 11069-11077, 10.1021/acs.est.8b02210, 2018.

Xu, R. C., Thornton, J. A., Lee, B., Zhang, Y. X., Jaegle, L., Lopez-Hilfiker, F. D., Rantala, P., and Petaja, T.: Global simulations of monoterpene-derived peroxy radical fates and the distributions of highly oxygenated organic molecules (HOMs) and accretion products, Atmos. Chem. Phys., 22, 5477-5494, 10.5194/acp-22-5477-2022, 2022.

Jokinen, T., Berndt, T., Makkonen, R., Kerminen, V. M., Junninen, H., Paasonen, P., Stratmann, F., Herrmann, H., Guenther, A. B., Worsnop, D. R., Kulmala, M., Ehn, M., and Sipila, M.: Production of extremely low volatile organic compounds from biogenic emissions: Measured yields and atmospheric implications, P. Natl. Acad. Sci. USA, 112, 7123-7128, 10.1073/pnas.1423977112, 2015.

Lee, S., Shin, J. E., Yoon, R., Yoo, H., and Kim, S.: Annulation of O-silyl N,O-ketene acetals with alkynes for the synthesis of dihydropyridinones and its application in concise total synthesis of phenanthroindolizidine alkaloids, Front. Chem., 11, 1267422, 10.3389/fchem.2023.1267422, 2023.

Liu, Y., Dong, X., Wang, M., Xu, R., Thornton, J. A., Shao, X., Emmons, L. K., Jo, D. S., Yue, M., and Shrivastava, M.: A Modeling Study of Global Distribution and Formation Pathways of Highly Oxygenated Organic Molecules Derived Secondary Organic Aerosols (HOMs-SOA) from Monoterpenes, J. Geophys. Res.-Atmos., (under review), 2024.

Pye, H. O. T., D'Ambro, E. L., Lee, B. H., Schobesberger, S., Takeuchi, M., Zhao, Y., Lopez-Hilfiker, F., Liu, J., Shilling, J. E., Xing, J., Mathur, R., Middlebrook, A. M., Liao, J., Welti, A., Graus, M., Warneke, C., de Gouw, J. A., Holloway, J. S., Ryerson, T. B., Pollack, I. B., and Thornton, J. A.: Anthropogenic enhancements to production of highly oxygenated molecules from autoxidation, P. Natl. Acad. Sci. USA, 116, 6641-6646, 10.1073/pnas.1810774116, 2019.

Roldin, P., Ehn, M., Kurtén, T., Olenius, T., Rissanen, M. P., Sarnela, N., Elm, J., Rantala, P., Hao, L., Hyttinen, N., Heikkinen, L., Worsnop, D. R., Pichelstorfer, L., Xavier, C., Clusius, P., Öström, E., Petäjä, T., Kulmala, M., Vehkamäki, H., Virtanen, A., Riipinen, I., and Boy, M.: The role of highly oxygenated organic molecules in the Boreal aerosol-cloud-climate system, Nat.Commun., 10, 4370, 10.1038/s41467-019-12338-8, 2019.

Weber, J., Archer-Nicholls, S., Griffiths, P., Berndt, T., Jenkin, M., Gordon, H., Knote, C., and Archibald, A. T.: CRI-HOM: A novel chemical mechanism for simulating highly oxygenated organic

molecules (HOMs) in global chemistry–aerosol–climate models, Atmos. Chem. Phys., 20, 10889-10910, 10.5194/acp-20-10889-2020, 2020.

Xu, L., Pye, H. O. T., He, J., Chen, Y., Murphy, B. N., and Ng, N. L.: Experimental and model estimates of the contributions from biogenic monoterpenes and sesquiterpenes to secondary organic aerosol in the southeastern United States, Atmos. Chem. Phys., 18, 12613-12637, 10.5194/acp-18-12613-2018, 2018.

Major Comment#2: Additionally, Liu et al (2024) identifies the branching in the NO termination pathway as being highly uncertain, but here the sensitivity to the rate of NO reaction is investigated. Why was the sensitivity to the rate rather than the branching ratio studied?

Response: In Liu et al. (2024), the adjustment of the branching ratio from 0.4 to 0 in the NO termination pathway of HOMs is based on significant uncertainties in this parameter (Weber et al., 2020; Roldin et al., 2019; Xu et al., 2022). Although this adjustment indeed alleviates the overestimation of HOMs concentrations at the Centreville and SMEAR II site (Fig. 2 in Liu et al., 2024, see below), it results in non-conservation of carbon atoms between reactants and products since the reaction changes from "MT-HOM-RO_2 + NO → 0.8*NO_2 + 0.8*HO_2 + 0.4*SOAGhmb + 0.8*HYDRALD + 0.2*SOAGhmn" to "MT-HOM-RO_2 + NO → 0.8*NO_2 + 0.8*HO_2 + 0.8*HYDRALD + 0.2*SOAGhmn", where MT-HOM-RO_2 is the multi-generation products of autoxidation, SOAGhmb and SOAGhmn are the gas phase C10-HOMs and HYDRALD is the lumped unsaturated hydroxycarbonyl (details of this reaction are shown in Table S2 in the response of minor comments 3 and 13).

Consequently, considering the overestimation of NO concentrations by a factor of five at Centreville and SMEAR II station, we adjusted the rate of the NO termination pathway to one-fifth of its original value to assess its impact on HOM concentrations as well as NPF rate. Also, adjusting the reaction rate to 20% of the original value is almost equivalent to adjusting the branching ratio from 0.4 to 0.08, which is very close to the experiment designed by Liu et al. (2024) (the branching ratio of HOMs is set as zero).

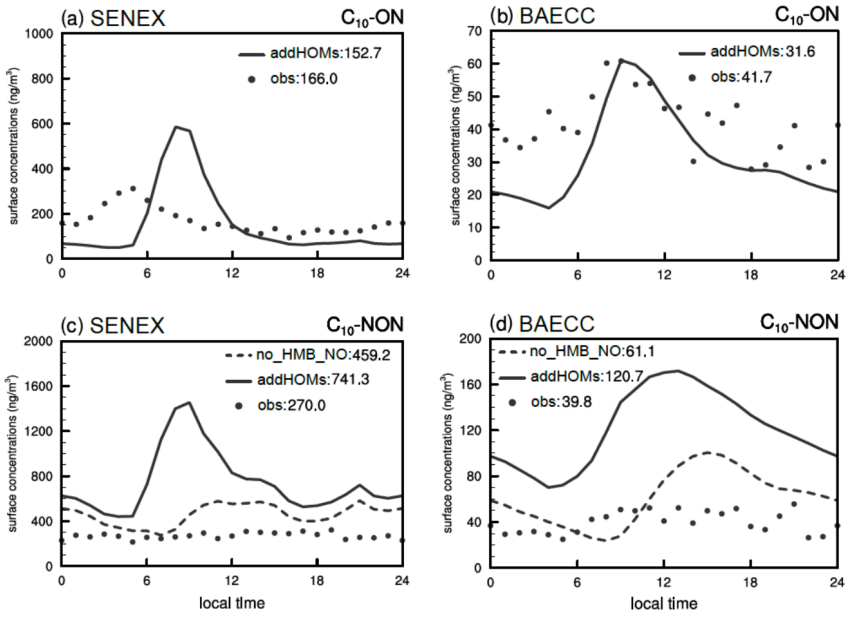

Figure. 2 in Liu et al., 2024: The diurnal cycle of observed (dots) surface C10-ON (a, b) and C10-NON (c, d) concentrations (unit: ng/m3) at the Centreville site during the SENEX campaign (a, c) and the SMEAR II sites during the BAECC (b, d) campaign. The simulated surface C10 HOMs (C10-ON and C10-NON) concentrations at the closest grid to the Centreville and the SMEAR II sites are used from the addHOMs (solid lines) and no_HMB_NO (dashed lines) experiments. The simulated C10 HOMs at two sites are scaled by the ratios of the observed monoterpene concentrations to the simulated monoterpene concentrations. AddHOMs is the basic experiments when adding HOMs chemistry and partitioning and no_HMB_NO is the experiments adjusting the yield of SOAGhmb as zero in NO termination pathway.

Reference

Liu, Y., Dong, X., Wang, M., Xu, R., Thornton, J. A., Shao, X., Emmons, L. K., Jo, D. S., Yue, M., and Shrivastava, M.: A Modeling Study of Global Distribution and Formation Pathways of Highly Oxygenated Organic Molecules Derived Secondary Organic Aerosols (HOMs-SOA) from Monoterpenes, J. Geophys. Res.-Atmos., (under review), 2024.

Roldin, P., Ehn, M., Kurtén, T., Olenius, T., Rissanen, M. P., Sarnela, N., Elm, J., Rantala, P., Hao, L., Hyttinen, N., Heikkinen, L., Worsnop, D. R., Pichelstorfer, L., Xavier, C., Clusius, P., Öström, E., Petäjä, T., Kulmala, M., Vehkamäki, H., Virtanen, A., Riipinen, I., and Boy, M.: The role of highly oxygenated organic molecules in the Boreal aerosol-cloud-climate system, Nat.Commun., 10, 4370, 10.1038/s41467-019-12338-8, 2019.

Weber, J., Archer-Nicholls, S., Griffiths, P., Berndt, T., Jenkin, M., Gordon, H., Knote, C., and Archibald, A. T.: CRI-HOM: A novel chemical mechanism for simulating highly oxygenated organic molecules (HOMs) in global chemistry–aerosol–climate models, Atmos. Chem. Phys., 20, 10889-10910, 10.5194/acp-20-10889-2020, 2020.

Xu, R. C., Thornton, J. A., Lee, B., Zhang, Y. X., Jaegle, L., Lopez-Hilfiker, F. D., Rantala, P., and Petaja, T.: Global simulations of monoterpene-derived peroxy radical fates and the distributions of highly oxygenated organic molecules (HOMs) and accretion products, Atmos. Chem. Phys., 22, 5477-5494, 10.5194/acp-22-5477-2022, 2022.

Major Comment#3 and #4: In Table 1, it is shown that all C20 and C15 compounds are represented by one species each with one volatility each. As seen in previous work (Stolzenburg 2018, Ye et al 2018, Schervish and Donahue 2020, etc.) not all accretion products lead to ULVOCs or even ELVOCs. The assumption that they do seems like it would dramatically overestimate the role of organic nucleation and growth.

While the low branching ratio to accretion products may somewhat account for the concern brought up in point 3, experimentally many C20s end up in the E/LVOC range, allowing them to contribute to small particle growth, and the mechanism seems to indicate products from C10+C10 accretion reactions can only be C20 ULVOCs or non-HOM species.

Response: Yes, the lack of consideration for C15 and C20 dimers in LVOCs and C20 dimers in ELVOCs is a limitation of the current chemical mechanism we used in CAM6-Chem. We appreciate the referee for providing some articles which showed the molecular formulas and concentration of accretion product in different volatility bins. But the explicit chemical kinetics of related reactions (i.e. the intermediate products and their yields) are not displayed. Therefore, we are unable to represent all the final products mentioned in these articles in the CAM6-Chem model.

However, we realize that this uncertainty is important and should be thoroughly discussed. Therefore, we have added the following discussion at the end of the **Summary**:

"There might be some overestimations with C15 and C20 involved in new particle formation if we assume that all the accretion products are ELVOC or ULVOC. In the updated model, $C_{15}H_{18}O_9$ (C15, extremely low volatility) and $C_{20}H_{32}O_8$ (C20, ultra-low volatility) are just simplified representatives of all C15 and C20 dimers. Although more dimer species with low volatility has been already detected on chamber experiments (Stolzenburg et al., 2018; Ye et al., 2018; Schervish and Donahue, 2020), they did not provide the explicit chemical kinetics of related reactions (i.e. the intermediate products and their yields). On the other hand, although yields of accretion products vary by 1 to 2 orders of magnitude in previous studies (Rissanen et al., 2015; Berndt et al., 2018; Zhao et al., 2018), the yields of C15 and C20 we currently use are very low (4%), resulting in relatively low dimer concentrations.

Even if they were all ELVOC and ULVOC, it would not lead to significant overestimation, and therefore, would not substantially impact nucleation and growth rates."

Reference

Berndt, T., Mentler, B., Scholz, W., Fischer, L., Herrmann, H., Kulmala, M., and Hansel, A.: Accretion Product Formation from Ozonolysis and OH Radical Reaction of α-Pinene: Mechanistic Insight and the Influence of Isoprene and Ethylene, Environ. Sci. Technol., 52, 11069-11077, 10.1021/acs.est.8b02210, 2018.

Rissanen, M. P., Kurtén, T., Sipilä, M., Thornton, J. A., Kausiala, O., Garmash, O., Kjaergaard, H. G., Petäjä, T., Worsnop, D. R., Ehn, M., and Kulmala, M.: Effects of Chemical Complexity on the Autoxidation Mechanisms of Endocyclic Alkene Ozonolysis Products: From Methylcyclohexenes toward Understanding α-Pinene, J. Phys. Chem. A, 119, 4633-4650, 10.1021/jp510966g, 2015.

Schervish, M. and Donahue, N. M.: Peroxy radical chemistry and the volatility basis set, Atmospheric Chemistry and Physics, 20, 1183-1199, 10.5194/acp-20-1183-2020, 2020.

Stolzenburg, D., Fischer, L., Vogel, A. L., Heinritzi, M., Schervish, M., Simon, M., Wagner, A. C., Dada, L., Ahonen, L. R., Amorim, A., Baccarini, A., Bauer, P. S., Baumgartner, B., Bergen, A., Bianchi, F., Breitenlechner, M., Brilke, S., Buenrostro Mazon, S., Chen, D., Dias, A., Draper, D. C., Duplissy, J., El Haddad, I., Finkenzeller, H., Frege, C., Fuchs, C., Garmash, O., Gordon, H., He, X., Helm, J., Hofbauer, V., Hoyle, C. R., Kim, C., Kirkby, J., Kontkanen, J., Kürten, A., Lampilahti, J., Lawler, M., Lehtipalo, K., Leiminger, M., Mai, H., Mathot, S., Mentler, B., Molteni, U., Nie, W., Nieminen, T., Nowak, J. B., Ojdanic, A., Onnela, A., Passananti, M., Petäjä, T., Quéléver, L. L. J., Rissanen, M. P., Sarnela, N., Schallhart, S., Tauber, C., Tomé, A., Wagner, R., Wang, M., Weitz, L., Wimmer, D., Xiao, M., Yan, C., Ye, P., Zha, Q., Baltensperger, U., Curtius, J., Dommen, J., Flagan, R. C., Kulmala, M., Smith, J. N., Worsnop, D. R., Hansel, A., Donahue, N. M., and Winkler, P. M.: Rapid growth of organic aerosol nanoparticles over a wide tropospheric temperature range, P. Natl. Acad. Sci. USA, 115, 9122-9127, 10.1073/pnas.1807604115, 2018.

Ye, Q., Wang, M., Hofbauer, V., Stolzenburg, D., Chen, D., Schervish, M., Vogel, A., Mauldin, R. L., Baalbaki, R., Brilke, S., Dada, L., Dias, A., Duplissy, J., El Haddad, I., Finkenzeller, H., Fischer, L., He, X., Kim, C., Kürten, A., Lamkaddam, H., Lee, C. P., Lehtipalo, K., Leiminger, M., Manninen, H. E., Marten, R., Mentler, B., Partoll, E., Petäjä, T., Rissanen, M., Schobesberger, S., Schuchmann, S., Simon, M., Tham, Y. J., Vazquez-Pufleau, M., Wagner, A. C., Wang, Y., Wu, Y., Xiao, M., Baltensperger, U., Curtius, J., Flagan, R., Kirkby, J., Kulmala, M., Volkamer, R., Winkler, P. M., Worsnop, D., and Donahue, N. M.: Molecular Composition and Volatility of Nucleated Particles from

α-Pinene Oxidation between −50 °C and +25 °C, Environ. Sci. Technol., 53, 12357-12365, 10.1021/acs.est.9b03265, 2019.

Zhao, Y., Thornton, J. A., and Pye, H. O. T.: Quantitative constraints on autoxidation and dimer formation from direct probing of monoterpene-derived peroxy radical chemistry, P. Natl. Acad. Sci. USA, 115, 12142-12147, 10.1073/pnas.1812147115, 2018.

Major Comment#5: Why are only 2 steps of autoxidation simulated? Laboratory evidence (Heinritzi et al 2020, Simon et al 2020, etc.) shows products with very high oxygen content that likely underwent more than 2 steps of autoxidation. Would allowing more autoxidation lead to a higher organic contribution to nucleation, or perhaps this model step up could suggest how many steps are likely to occur in the actual atmosphere prior to termination or condensation.

Response: Currently, two-step autoxidation reactions are used to approximately represent the formation of C10-HOMs undergoing multiple steps of autoxidation reactions (more than one step). As mentioned in Heinritzi et al. (2020), three steps of autoxidation products were reported (i.e., $C_{10}H_{15}O_{4,\ 6,\ 8,\ 10}$ radicals) in chamber experiments yet more than three generations might occur. Additionally, Heinritzi et al. (2020) and Simon et al. (2020) did not provide the chemical reaction and reaction rates for multi-step oxidation products. So in the model we use two steps to approximate multi-generation.

We appreciate the referee for reminding on this important issue and this uncertainty should be thoroughly discussed, so we have added the following discussion at the end of the **Summary**:

"Although we only consider two-step autoxidation reactions which is not the most advanced (Heinritzi et al., 2020; Simon et al., 2020), its impact on organic nucleation rate is almost negligible. The number of autoxidation steps has almost no effect on the rate of heteromolecular nucleation of sulfuric acid and organics (HET), which is the most significant contributors to organic nucleation rate (Fig. 6 in the main text). This is mainly because the number of autoxidation steps affects neither the yield nor the concentration of C10-HOMs, only their molecular formulas and volatility. In our simulation, the lower volatility of C10-HOMs does not affect their participation in HET (i.e. LVOC, ELVOC and ULVOC can all contribute to HET), so the rate of HET is not influenced by the number of autoxidation step.

C10-HOMs might become less volatile when undergoing one additional autoxidation step, transitioning from LVOC ($3 \times 10^{-5} < C^*(T) < 0.3$ μg m^{-3}, where $C^*(T)$ is the effective saturation concentration) to ELVOC ($3 \times 10^{-9} < C^*(T) < 3 \times 10^{-5}$ μg m^{-3}), but this is unlikely to affect the pure

organic nucleation rate. The is because previous studies (Kurtén et al., 2016; Tröstl et al., 2016) have already indicated that C10 class molecules alone do not have low enough vapor pressure to initiate the nucleation, without the presence of other species such as sulfuric acid or bases. This is further supported by that C20 class molecules are mainly responsible for pure biogenic nucleation (Heinritzi et al 2020; Frege et al., 2018)."

In Heinritzi et al. (2020), the chain of α-Pinene RO_2 mostly consists of $C_{10}H_{15}O_{4,\ 6,\ 8,\ 10}$ radicals, this does not mean only three steps autoxidation occurring in the real atmosphere. Therefore, we are not able to set up the number of autoxidation steps before termination or condensation.

Reference

Frege, C., Ortega, I. K., Rissanen, M. P., Praplan, A. P., Steiner, G., Heinritzi, M., Ahonen, L., Amorim, A., Bernhammer, A. K., Bianchi, F., Brilke, S., Breitenlechner, M., Dada, L., Dias, A., Duplissy, J., Ehrhart, S., El-Haddad, I., Fischer, L., Fuchs, C., Garmash, O., Gonin, M., Hansel, A., Hoyle, C. R., Jokinen, T., Junninen, H., Kirkby, J., Kurten, A., Lehtipalo, K., Leiminger, M., Mauldin, R. L., Molteni, U., Nichman, L., Petaja, T., Sarnela, N., Schobesberger, S., Simon, M., Sipila, M., Stolzenburg, D., Tome, A., Vogel, A. L., Wagner, A. C., Wagner, R., Xiao, M., Yan, C., Ye, P. L., Curtius, J., Donahue, N. M., Flagan, R. C., Kulmala, M., Worsnop, D. R., Winkler, P. M., Dommen, J., and Baltensperger, U.: Influence of temperature on the molecular composition of ions and charged clusters during pure biogenic nucleation, Atmospheric Chemistry and Physics, 18, 65-79, 10.5194/acp-18-65-2018, 2018.

Heinritzi, M., Dada, L., Simon, M., Stolzenburg, D., Wagner, A. C., Fischer, L., Ahonen, L. R., Amanatidis, S., Baalbaki, R., Baccarini, A., Bauer, P. S., Baumgartner, B., Bianchi, F., Brilke, S., Chen, D., Chiu, R., Dias, A., Dommen, J., Duplissy, J., Finkenzeller, H., Frege, C., Fuchs, C., Garmash, O., Gordon, H., Granzin, M., El Haddad, I., He, X., Helm, J., Hofbauer, V., Hoyle, C. R., Kangasluoma, J., Keber, T., Kim, C., Kürten, A., Lamkaddam, H., Laurila, T. M., Lampilahti, J., Lee, C. P., Lehtipalo, K., Leiminger, M., Mai, H., Makhmutov, V., Manninen, H. E., Marten, R., Mathot, S., Mauldin, R. L., Mentler, B., Molteni, U., Müller, T., Nie, W., Nieminen, T., Onnela, A., Partoll, E., Passananti, M., Petäjä, T., Pfeifer, J., Pospisilova, V., Quéléver, L. L. J., Rissanen, M. P., Rose, C., Schobesberger, S., Scholz, W., Scholze, K., Sipilä, M., Steiner, G., Stozhkov, Y., Tauber, C., Tham, Y. J., Vazquez-Pufleau, M., Virtanen, A., Vogel, A. L., Volkamer, R., Wagner, R., Wang, M., Weitz, L., Wimmer, D., Xiao, M., Yan, C., Ye, P., Zha, Q., Zhou, X., Amorim, A., Baltensperger, U., Hansel, A., Kulmala, M., Tomé, A., Winkler, P. M., Worsnop, D. R., Donahue, N. M., Kirkby, J., and Curtius, J.: Molecular understanding of the suppression of new-particle formation by isoprene, Atmos. Chem. Phys., 20, 11809-11821, 10.5194/acp-20-11809-2020, 2020.

Kurtén, T., Tiusanen, K., Roldin, P., Rissanen, M., Luy, J.-N., Boy, M., Ehn, M., and Donahue, N.: α-Pinene Autoxidation Products May Not Have Extremely Low Saturation Vapor Pressures Despite High O:C Ratios, J. Phys. Chem. A, 120, 2569-2582, 10.1021/acs.jpca.6b02196, 2016.

Simon, M., Dada, L., Heinritzi, M., Scholz, W., Stolzenburg, D., Fischer, L., Wagner, A. C., Kürten, A., Rörup, B., He, X. C., Almeida, J., Baalbaki, R., Baccarini, A., Bauer, P. S., Beck, L., Bergen, A., Bianchi, F., Bräkling, S., Brilke, S., Caudillo, L., Chen, D., Chu, B., Dias, A., Draper, D. C., Duplissy, J., El-Haddad, I., Finkenzeller, H., Frege, C., Gonzalez-Carracedo, L., Gordon, H., Granzin, M., Hakala, J., Hofbauer, V., Hoyle, C. R., Kim, C., Kong, W., Lamkaddam, H., Lee, C. P., Lehtipalo, K., Leiminger, M., Mai, H., Manninen, H. E., Marie, G., Marten, R., Mentler, B., Molteni, U., Nichman, L., Nie, W., Ojdanic, A., Onnela, A., Partoll, E., Petäjä, T., Pfeifer, J., Philippov, M., Quéléver, L. L. J., Ranjithkumar, A., Rissanen, M. P., Schallhart, S., Schobesberger, S., Schuchmann, S., Shen, J., Sipilä, M., Steiner, G., Stozhkov, Y., Tauber, C., Tham, Y. J., Tomé, A. R., Vazquez-Pufleau, M., Vogel, A. L., Wagner, R., Wang, M., Wang, D. S., Wang, Y., Weber, S. K., Wu, Y., Xiao, M., Yan, C., Ye, P., Ye, Q., Zauner-Wieczorek, M., Zhou, X., Baltensperger, U., Dommen, J., Flagan, R. C., Hansel, A., Kulmala, M., Volkamer, R., Winkler, P. M., Worsnop, D. R., Donahue, N. M., Kirkby, J., and Curtius, J.: Molecular understanding of new-particle formation from α-pinene between −50 and +25 °C, Atmos. Chem. Phys., 20, 9183-9207, 10.5194/acp-20-9183-2020, 2020.

Trostl, J., Chuang, W. K., Gordon, H., Heinritzi, M., Yan, C., Molteni, U., Ahlm, L., Frege, C., Bianchi, F., Wagner, R., Simon, M., Lehtipalo, K., Williamson, C., Craven, J. S., Duplissy, J., Adamov, A., Almeida, J., Bernhammer, A. K., Breitenlechner, M., Brilke, S., Dias, A., Ehrhart, S., Flagan, R. C., Franchin, A., Fuchs, C., Guida, R., Gysel, M., Hansel, A., Hoyle, C. R., Jokinen, T., Junninen, H., Kangasluoma, J., Keskinen, H., Kim, J., Krapf, M., Kurten, A., Laaksonen, A., Lawler, M., Leiminger, M., Mathot, S., Mohler, O., Nieminen, T., Onnela, A., Petaja, T., Piel, F. M., Miettinen, P., Rissanen, M. P., Rondo, L., Sarnela, N., Schobesberger, S., Sengupta, K., Sipila, M., Smith, J. N., Steiner, G., Tome, A., Virtanen, A., Wagner, A. C., Weingartner, E., Wimmer, D., Winkler, P. M., Ye, P. L., Carslaw, K. S., Curtius, J., Dommen, J., Kirkby, J., Kulmala, M., Riipinen, I., Worsnop, D. R., Donahue, N. M., and Baltensperger, U.: The role of low-volatility organic compounds in initial particle growth in the atmosphere, Nature, 533, 527-+, 10.1038/nature18271, 2016.

Major Comment#6: Are any particle-phase processing of HOMs considered such as particle phase oligomerization or decomposition of accretion products and organic hydroperoxides?

Response: Particle phase oligomerization or decomposition were not taken into considered in our updated model. One reason is that the default version of CAM-Chem did not include these process (Jo et al., 2023). Also, compared to particle phase, we are more focused on the process that may affect the concentration of gaseous HOMs. Additionally, the deposition and photolysis of particle phase HOMs were added in our model.

However, we think it is necessary to discuss the uncertainties arising from disregarding these processes, and we have added the following content to the discussion of uncertainties in the **Summary**:

"Neglecting the oligomerization of accretion products can lead to higher volatility of aerosols, resulting in reduced the mass concentration in the particle phase and reduced condensation sink (CS), but increased mass in the gaseous phase. This could lead to an overestimation of the NPF rate. However, since the mass of HOMs-SOA accounts for only about 10% of the total SOA mass, the impact on NPF rate can be neglected.

Not considering decomposition of accretion products may lead to an overestimation of the mass and number concentration of HOMs in particle phase, and consequently an overestimation of CS and underestimation of the NPF rate. However, C15-SOA and C20-SOA account for less than 4% of the total SOA (Liu et al., 2024), so the impact of ignoring the decomposition of accretion products is negligible."

In our model, organic hydroperoxides are in gaseous phase so we did not consider decomposition of organic hydroperoxides. Since the intermediate RO_2 lifetime will rarely exceed about 100 s (Bianchi et al., 2018), the impact of ignoring its decomposition on NPF rate is minimal.

Reference

Bianchi, F., Kurten, T., Riva, M., Mohr, C., Rissanen, M. P., Roldin, P., Berndt, T., Crounse, J. D., Wennberg, P. O., Mentel, T. F., Wildt, J., Junninen, H., Jokinen, T., Kulmala, M., Worsnop, D. R., Thornton, J. A., Donahue, N., Kjaergaard, H. G., and Ehn, M.: Highly Oxygenated Organic Molecules (HOM) from Gas-Phase Autoxidation Involving Peroxy Radicals: A Key Contributor to Atmospheric Aerosol, Chem. Rev., 119, 3472-3509, 10.1021/acs.chemrev.8b00395, 2019.

Jo, Y., Jang, M., Han, S., Madhu, A., Koo, B., Jia, Y., Yu, Z., Kim, S., and Park, J.: CAMx-UNIPAR Simulation of SOA Mass Formed from Multiphase Reactions of Hydrocarbons under the Central Valley Urban Atmospheres of California, EGUsphere, 2023, 1-30, 10.5194/egusphere-2023-93, 2023.

Liu, Y., Dong, X., Wang, M., Xu, R., Thornton, J. A., Shao, X., Emmons, L. K., Jo, D. S., Yue, M., and Shrivastava, M.: A Modeling Study of Global Distribution and Formation Pathways of Highly Oxygenated Organic Molecules Derived Secondary Organic Aerosols (HOMs-SOA) from Monoterpenes, J. Geophys. Res.-Atmos., (under review), 2024.

Major Comment#7: In Liu et al (2024), it seems that the HOM chemistry mechanism overpredicts surface HOM mass concentrations. While, I agree with the argument in that work that this could be due to limited detection of HOMs in the observations, more recent lab work (including Stolzenburg et al 2018 referenced earlier) has focused on closing that gap and could be simulated as well. It seems difficult to justify moving forward in the current work with this mechanism without more thorough validation.

Response: We agree with the referee that more observation data is highly demanded to validate this mechanism. Yet it shall be mentioned that the measurements derived from previous studies (Stolzenburg et al., 2018; Ye et al., 2018; Schervish and Donahue,2020) are usually not comparable with global model. Most of the chamber measurements indeed provide detailed information regarding HOMs in each volatility bin, but chamber experiments were configured with certain meteorology conditions that greatly differ from modeled real atmospheric conditions, and it is also difficult for chamber experiments to consider the dynamics of other processes such as emission and transport. So in this study we prefer to employ field measurements for model validation, despite the limited data.

In addition, CAM6-Chem was run at a horizontal resolution of 0.95° latitude and 1.25° longitude (~111 km), so we need long-term observational data for comparison. The measurement data we used are from the Southeast Nexus (SENEX; Warneke et al., 2016) and Biogenic Aerosols-Effects on Clouds and Climate (BAECC; Petäjä et al., 2016) field campaigns, which are nearly the most thorough long-term field observational data we can obtain. Although recent studies have provided concentrations of organic oxygenated molecules (OOMs) from field observations (Qiao et al., 2021; Guo et al., 2022; Nie et al., 2022), these measurements are concentrated in megacities so most of the OOM components are anthropogenic and cannot be used to compare with the biogenic-HOMs concentrations we simulate.

Reference

Schervish, M. and Donahue, N. M.: Peroxy radical chemistry and the volatility basis set, Atmospheric Chemistry and Physics, 20, 1183-1199, 10.5194/acp-20-1183-2020, 2020.

Stolzenburg, D., Fischer, L., Vogel, A. L., Heinritzi, M., Schervish, M., Simon, M., Wagner, A. C., Dada, L., Ahonen, L. R., Amorim, A., Baccarini, A., Bauer, P. S., Baumgartner, B., Bergen, A., Bianchi, F., Breitenlechner, M., Brilke, S., Buenrostro Mazon, S., Chen, D., Dias, A., Draper, D. C., Duplissy, J., El Haddad, I., Finkenzeller, H., Frege, C., Fuchs, C., Garmash, O., Gordon, H., He, X., Helm, J., Hofbauer, V., Hoyle, C. R., Kim, C., Kirkby, J., Kontkanen, J., Kürten, A., Lampilahti, J., Lawler, M., Lehtipalo, K., Leiminger, M., Mai, H., Mathot, S., Mentler, B., Molteni, U., Nie, W., Nieminen, T., Nowak, J. B., Ojdanic, A., Onnela, A., Passananti, M., Petäjä, T., Quéléver, L. L. J., Rissanen, M. P., Sarnela, N., Schallhart, S., Tauber, C., Tomé, A., Wagner, R., Wang, M., Weitz, L., Wimmer, D., Xiao, M., Yan, C., Ye, P., Zha, Q., Baltensperger, U., Curtius, J., Dommen, J., Flagan, R. C., Kulmala, M., Smith, J. N., Worsnop, D. R., Hansel, A., Donahue, N. M., and Winkler, P. M.: Rapid growth of organic aerosol nanoparticles over a wide tropospheric temperature range, P. Natl. Acad. Sci. USA, 115, 9122-9127, 10.1073/pnas.1807604115, 2018.

Ye, Q., Wang, M., Hofbauer, V., Stolzenburg, D., Chen, D., Schervish, M., Vogel, A., Mauldin, R. L., Baalbaki, R., Brilke, S., Dada, L., Dias, A., Duplissy, J., El Haddad, I., Finkenzeller, H., Fischer, L., He, X., Kim, C., Kürten, A., Lamkaddam, H., Lee, C. P., Lehtipalo, K., Leiminger, M., Manninen, H. E., Marten, R., Mentler, B., Partoll, E., Petäjä, T., Rissanen, M., Schobesberger, S., Schuchmann, S., Simon, M., Tham, Y. J., Vazquez-Pufleau, M., Wagner, A. C., Wang, Y., Wu, Y., Xiao, M., Baltensperger, U., Curtius, J., Flagan, R., Kirkby, J., Kulmala, M., Volkamer, R., Winkler, P. M., Worsnop, D., and Donahue, N. M.: Molecular Composition and Volatility of Nucleated Particles from α-Pinene Oxidation between −50 °C and +25 °C, Environ. Sci. Technol., 53, 12357-12365, 10.1021/acs.est.9b03265, 2019.

Petäjä, T., O'Connor, E. J., Moisseev, D., Sinclair, V. A., Manninen, A. J., Väänänen, R., von Lerber, A., Thornton, J. A., Nicoll, K., Petersen, W., Chandrasekar, V., Smith, J. N., Winkler, P. M., Krüger, O., Hakola, H., Timonen, H., Brus, D., Laurila, T., Asmi, E., Riekkola, M.-L., Mona, L., Massoli, P., Engelmann, R., Komppula, M., Wang, J., Kuang, C., Bäck, J., Virtanen, A., Levula, J., Ritsche, M., and Hickmon, N.: BAECC: A Field Campaign to Elucidate the Impact of Biogenic Aerosols on Clouds and Climate, Bull. Amer. Meteor. Soc., 97, 1909-1928, https://doi.org/10.1175/BAMS-D-14-00199.1, 2016.

Warneke, C., Trainer, M., de Gouw, J. A., Parrish, D. D., Fahey, D. W., Ravishankara, A. R., Middlebrook, A. M., Brock, C. A., Roberts, J. M., Brown, S. S., Neuman, J. A., Lerner, B. M., Lack, D., Law, D., Hübler, G., Pollack, I., Sjostedt, S., Ryerson, T. B., Gilman, J. B., Liao, J., Holloway, J., Peischl, J., Nowak, J. B., Aikin, K. C., Min, K. E., Washenfelder, R. A., Graus, M. G., Richardson, M., Markovic, M. Z., Wagner, N. L., Welti, A., Veres, P. R., Edwards, P., Schwarz, J. P., Gordon, T., Dube, W. P., McKeen, S. A., Brioude, J., Ahmadov, R., Bougiatioti, A., Lin, J. J., Nenes, A., Wolfe,

G. M., Hanisco, T. F., Lee, B. H., Lopez-Hilfiker, F. D., Thornton, J. A., Keutsch, F. N., Kaiser, J., Mao, J., and Hatch, C. D.: Instrumentation and measurement strategy for the NOAA SENEX aircraft campaign as part of the Southeast Atmosphere Study 2013, Atmos. Meas. Tech., 9, 3063-3093, 10.5194/amt-9-3063-2016, 2016.

Qiao, X., Yan, C., Li, X., Guo, Y., Yin, R., Deng, C., Li, C., Nie, W., Wang, M., Cai, R., Huang, D., Wang, Z., Yao, L., Worsnop, D. R., Bianchi, F., Liu, Y., Donahue, N. M., Kulmala, M., and Jiang, J.: Contribution of Atmospheric Oxygenated Organic Compounds to Particle Growth in an Urban Environment, Environ. Sci. Technol., 55, 13646-13656, 10.1021/acs.est.1c02095, 2021.

Guo, Y., Yan, C., Liu, Y., Qiao, X., Zheng, F., Zhang, Y., Zhou, Y., Li, C., Fan, X., Lin, Z., Feng, Z., Zhang, Y., Zheng, P., Tian, L., Nie, W., Wang, Z., Huang, D., Daellenbach, K. R., Yao, L., Dada, L., Bianchi, F., Jiang, J., Liu, Y., Kerminen, V. M., and Kulmala, M.: Seasonal variation in oxygenated organic molecules in urban Beijing and their contribution to secondary organic aerosol, Atmos. Chem. Phys., 22, 10077-10097, 10.5194/acp-22-10077-2022, 2022.

Nie, W., Yan, C., Huang, D. D., Wang, Z., Liu, Y. L., Qiao, X. H., Guo, Y. S., Tian, L. H., Zheng, P. G., Xu, Z. N., Li, Y. Y., Xu, Z., Qi, X. M., Sun, P., Wang, J. P., Zheng, F. X., Li, X. X., Yin, R. J., Dallenbach, K. R., Bianchi, F., Petaja, T., Zhang, Y. J., Wang, M. Y., Schervish, M., Wang, S. N., Qiao, L. P., Wang, Q., Zhou, M., Wang, H. L., Yu, C. A., Yao, D. W., Guo, H., Ye, P. L., Lee, S. C., Li, Y. J., Liu, Y. C., Chi, X. G., Kerminen, V. M., Ehn, M., Donahue, N. M., Wang, T., Huang, C., Kulmala, M., Worsnop, D., Jiang, J. K., and Ding, A. J.: Secondary organic aerosol formed by condensing anthropogenic vapours over China's megacities, Nature Geoscience, 15, 255-+, 10.1038/s41561-022-00922-5, 2022.

Major Comment#8: Overall, I think much more discussion needs to be provided into what the uncertainties in this model are and how they limit the abilities and applications of this mechanism in the context of this paper. For example, Liu et al (2024) finds that temperature is a significant parameter affecting HOM formation, but this work does not discuss at all the temperature-dependence of autoxidation and how this uncertain parameter can affect the results in this work.

Response: Thank you for the suggestion. We have added a section (**Section 5**) to discuss the various potential uncertainties. The details are shown in the response for major comment#1.

Minor Comment#1: The title describes the chemical mechanism as "explicit." This to me indicates that you are representing the full chemistry with specific chemical species. However radical species are lumped leading to a reduced, perhaps, semi-explicit mechanism. I would consider editing the title to make that clearer.

Response: Thank you for the suggestion. We have modified this.

Minor Comment#2: Line 30-31: What does this sentence mean? I think this is referencing the finding that turning off organic initial growth leads to a greater decrease in the aerosol number, but the wording is very confusing.

Response: We apologize for the unclear description. The sentence at Line 30 is modified to "Compared to turning off the organic nucleation rate, turning off organic initial growth results in a more substantial decrease in aerosol number concentrations."

Minor Comment#3 and 13: A more detailed description of the mechanism should be provided with important assumptions made clear as a reference to another paper does not provide enough context.

If Liu et al (2024) is not published, please provide the full mechanism in this paper.

Response: We agree with the referee that an explicit list of the chemical reactions of HOMs would enhance the detail and clarity of our manuscript. Currently, the paper by Liu et al. (2024) that contains a comprehensive description of the mechanism is still under review. Consequently, we prefer not to transpose the same content to this manuscript. Nevertheless, to address the concern raised by the reviewers regarding our submission, we have added a succinct description of the machniasm that captures the essential details to the supplementary material in this revision, with a schematic figure and a list of representative chemical reactions. Furthermore, we have prepared a more thorough account of the complete chemical mechanism as outlined below:

Figure S1 shows a flowchart of the HOMs mechanism implemented into CAM6-Chem. In general, monoterpenes are oxidized by OH radicals or O_3 to form MT-aRO_2 and MT-bRO_2 radicals. MT-bRO_2 undergo multi-step autoxidation reactions to form HOMs with 10 carbon atoms (C10-HOMs) (green arrows in Fig. S1). The intermediates for the two-step autoxidation are MT-cRO_2 and MT-HOM-RO_2. The MT-HOM-RO_2 radical represents the RO_2 radicals that undergo two or multi-step autoxidation. On the one hand, MT-HOM-RO_2 radicals are further oxidized to form C10-HOMs. On the other hand,

all the MT-RO_2 radicals (including MT-aRO_2, MT-bRO_2, MT-cRO_2, and MT-HOM-RO_2) undergo self- and cross-reactions to form accretion products (C15 and C20) (orange arrows in Fig. S1). The formation processes of C10-HOMs can be terminated by several oxidants (gray arrows in Fig. S1). SOA is formed via gas-particle partitioning processes of C10-HOMs, C15 and C20 (blue dashed arrows in Fig. S1).

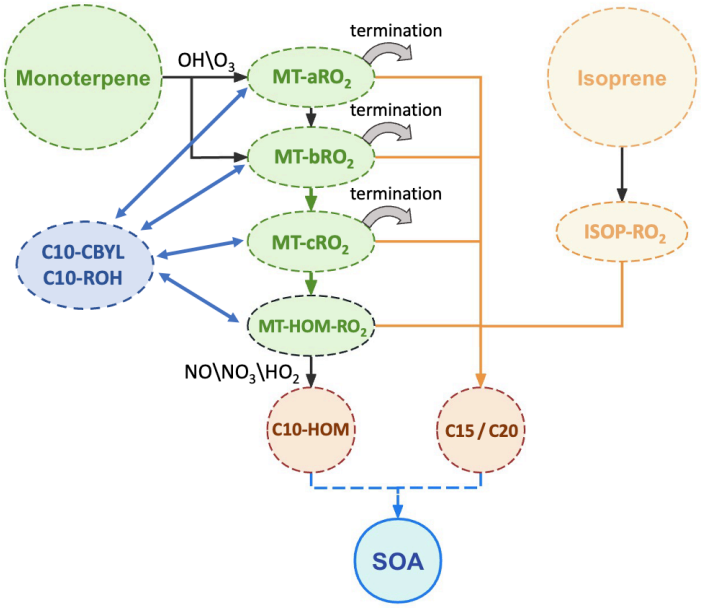

Figure S1. The flow chart of the formation and gas-particle partitioning processes of HOMs and accretion products. The green arrows represent the autoxidation reactions. The gray curved solid arrows represent the termination reactions. The yellow arrows represent the self- and cross-reactions. The blue arrows represent the conversion between C10-CBYL\C10-ROH and MT-RO_2 radicals. The blue dashed arrows represent the gas-particle partitioning processes.

The formation, photolysis, and scavenging processes of C10-HOMs C15 and C20 are detailed discussed as follows.

1. Monoterpene oxidation and autoxidation

Reaction 1-8 show the new branching which forms MT-bRO_2 that can undergo autoxidation are included in the original monoterpene + OH\O_3 reactions. The $APINO_2$, $BPINO_2$, $LIMONO_2$, and $MYRCO_2$ (MT-aRO_2) are the original formed RO_2 that cannot form HOMs. Reaction 9-10 show the MT-bRO_2 may go through two generations of autoxidation reaction (Table S1).

Table S1. Initial oxidation between monoterpenes and OH radical

Index	Reactions
1	APIN + OH → 0.25*$APINO_2$ + 0.75*MT-bRO_2
2	BPIN + OH → 0.25*$BPINO_2$ + 0.75*MT-bRO_2
3	LIMON + OH → 0.25*$LIMONO_2$ + 0.75*MT-bRO_2
4	MYRC + OH → 0.25*$MYRCO_2$ + 0.75*MT-bRO_2
5	APIN + O_3 → 0.736*$APINO_2$ + 0.064*MT-bRO_2 + 0.77*OH + 0.066*$TERPA2O_2$ + 0.22*H_2O_2 + 0.044*TERPA + 0.002*TERPACID + 0.034*TERPA2 + 0.17*HO_2 + 0.17*CO + 0.27*CH_2O + 0.054*$TERPA2CO_3$
6	BPIN + O_3 → 0.736*$BPINO_2$ + 0.064*MT-bRO_2 + 0.102*TERPK + 0.3*OH + 0.06*$TERPA2CO_3$ + 0.32*H_2O_2 + 0.038*BIGALK + 0.19*CO_2 + 0.81*CH_2O +0.11*HMHP + 0.08*HCOOH
7	LIMON + O_3 → 0.736*$LIMONO_2$ + 0.064*MT-bRO_2 + 0.66*OH + 0.132*TERPF1 + 0.33*CH_3CO_3 + 0.33*CH_2O + 0.066*$TERPA3CO_3$ + 0.33*H_2O_2 + 0.002*TERPACID
8	MYRC + O_3 → 0.736*$MYRCO_2$ + 0.064*MT-bRO_2 + 0.2*TERPF2 + 0.63*OH + 0.63*HO_2 + 0.25*CH_3COCH_3 +0.39*CH_2O + 0.18*HYAC
9	MT-bRO_2 → MT-cRO_2
10	MT-cRO_2 → MT-HOM-RO_2

2. Formation of C10-HOMs and accretion products

Reaction 11-24 show self- and cross-reactions of MT-RO_2 and ISOP-RO_2 to form accretion products (SOAGac15 and SOAGac20). Reaction 25-27 show the MT-HOM-RO_2 are oxidized by HO_2\NO\NO_3 to form C10-HOMs, including non-nitrate HOMs (SOAGhma and SOAGhmb) and nitrate HOMs (SOAGhmn) (Table S2).

Table S2. Self- and cross-reactions to form gas-phase accretion products

Index	Reactions
11	MT-aRO_2 + MT-aRO_2 → 0.893*C_{10}-CBYL + 0.29*C_{10}-ROH + 0.603*HO_2 + 1.34*HYDRALD + 0.067*MT-bRO_2 + 0.04*SOAGac20
12	MT-aRO_2 + MT-bRO_2 → 0.96*C_{10}-CBYL + 0.29*C_{10}-ROH + 0.67*HO_2 + 1.34*HYDRALD + 0.04*SOAGac20

13	MT-aRO$_2$ + MT-cRO$_2$ → 0.96*C$_{10}$-CBYL + 0.29*C$_{10}$-ROH + 0.67*HO$_2$ + 1.34*HYDRALD + 0.04*SOAGac20
14	MT-aRO$_2$ + MT-HOM-RO$_2$ → 0.96*C$_{10}$-CBYL + 0.29*C$_{10}$-ROH + 0.67*HO$_2$ + 1.34*HYDRALD + 0.04*SOAGac20
15	MT-aRO$_2$ + ISOP-RO$_2$ → 0.4465*C$_{10}$-CBYL + 0.145*C$_{10}$-ROH + 0.145*ROH + 0.603*HO$_2$ + 1.485*HYDRALD + 0.0335*MT-bRO$_2$ + 0.04*SOAGac15
16	MT-bRO$_2$ + MT-bRO$_2$ → 0.96*C$_{10}$-CBYL + 0.29*C$_{10}$-ROH + 0.67*HO$_2$ + 1.34*HYDRALD + 0.04*SOAGac20
17	MT-cRO$_2$ + MT-cRO$_2$ → 0.96*C$_{10}$-CBYL + 0.29*C$_{10}$-ROH + 0.67*HO$_2$ + 1.34*HYDRALD + 0.04*SOAGac20
18	MT-HOM-RO$_2$ + MT-HOM-RO$_2$ → 0.96*C$_{10}$-CBYL + 0.29*C$_{10}$-ROH + 0.67*HO$_2$ + 1.34*HYDRALD + 0.04*SOAGac20
19	MT-bRO$_2$ + MT-cRO$_2$ → 0.96*C$_{10}$-CBYL + 0.29*C$_{10}$-ROH + 0.67*HO$_2$ + 1.34*HYDRALD + 0.04*SOAGac20
20	MT-bRO$_2$ + MT-HOM-RO$_2$ → 0.96*C$_{10}$-CBYL + 0.29*C$_{10}$-ROH + 0.67*HO$_2$ + 1.34*HYDRALD + 0.04*SOAGac20
21	MT-cRO$_2$ + MT-HOM-RO$_2$ → 0.96*C$_{10}$-CBYL + 0.29*C$_{10}$-ROH + 0.67*HO$_2$ + 1.34*HYDRALD + 0.04*SOAGac20
22	MT-bRO$_2$ + ISOP-RO$_2$ → 0.48*C$_{10}$-CBYL + 0.145*C$_{10}$-ROH + 0.145*ROH + 0.67*HO$_2$ + 1.485*HYDRALD + 0.04*SOAGac15
23	MT-cRO$_2$ + ISOP-RO$_2$ → 0.48*C$_{10}$-CBYL + 0.145*C$_{10}$-ROH + 0.145*ROH + 0.67*HO$_2$ + 1.485*HYDRALD + 0.04*SOAGac15
24	MT-HOM-RO$_2$ + ISOP-RO$_2$ → 0.48*C$_{10}$-CBYL + 0.145*C$_{10}$-ROH + 0.145*ROH + 0.67*HO$_2$ + 1.485*HYDRALD + 0.04*SOAGac15
25	MT-HOM-RO$_2$ + HO$_2$ → SOAGhma + O$_2$
26	MT-HOM-RO$_2$ + NO → 0.8*NO$_2$ + 0.8*HO$_2$ + 0.4*SOAGhmb + 0.8*HYDRALD + 0.2*SOAGhmn
27	MT-HOM-RO$_2$ + NO$_3$ → HO$_2$ + NO$_2$ + 0.5*SOAGhmb + HYDRALD

3. Other reactions of MT-RO$_2$

Reaction 28-37 show MT-bRO$_2$, MT-cRO$_2$, and MT-HOM-RO$_2$ are terminated by methylperoxy/peroxyacetyl radicals. Reaction 38-49 show the MT-bRO$_2$\MT-cRO$_2$ reacts with NO/NO$_3$ (Table S3).

Table S3. MT-RO$_2$ reactions with methylperoxy/peroxyacetyl radicals

Index	Reactions
28	APINO$_2$ + CH$_3$CO$_3$ →

	0.05*MT-bRO$_2$ + 0.3705*TERPA + 0.3325*TERPA3 + 0.133*TERP1OOH + 0.12*CH$_3$COCH$_3$ + 0.114*TERPF1 + 0.27*CH$_2$O + HO$_2$ + CH$_3$O$_2$ + CO$_2$
29	APINO$_2$ + CH$_3$O$_2$ → 0.05*MT-bRO$_2$ + 0.83*CH$_2$O + 0.133*TERPF1 + 0.399*TERPA + 0.19*TERPA3 + 0.1235*TERP1OOH + 0.17*CH$_3$OH + 0.1045*TERPK + 0.06*CH$_3$COCH$_3$ + 1.16*HO$_2$
30	BPINO$_2$ + CH$_3$CO$_3$ → 0.05*MT-bRO$_2$ + 0.304*TERPK + 0.2565*TERPF1 + 0.3895*TERPA3 + 0.11*CH$_3$COCH$_3$ + 0.65*CH$_2$O + HO$_2$ + CH$_3$O$_2$ + CO$_2$
31	BPINO$_2$ + CH$_3$O$_2$ → 0.05*MT-bRO$_2$ + 1.4*CH$_2$O + 0.3515*TERPF1 + 0.304*TERPK + 1.5*HO$_2$ + 0.08*CH$_3$COCH$_3$ + 0.2945*TERPA3
32	LIMONO$_2$ + CH$_3$CO$_3$ → 0.05*MT-bRO$_2$ + 0.95*TERPF1 + 0.56*CH$_2$O + HO$_2$ + CH$_3$O$_2$ + CO$_2$
33	LIMONO$_2$ + CH$_3$O$_2$ → 0.05*MT-bRO$_2$ + 0.25*CH$_3$OH + 0.95*TERPF1 + 1.03*CH$_2$O + HO$_2$
34	MYRCO$_2$ + CH$_3$CO$_3$ → 0.05*MT-bRO$_2$ + 0.95*TERPF2 + HO$_2$ + 0.46*CH$_3$COCH$_3$ + 0.42*CH$_2$O + CH$_3$O$_2$ + CO$_2$
35	MYRCO$_2$ + CH$_3$O$_2$ → 0.05*MT-bRO$_2$ + 0.25*CH$_3$OH + 0.95*TERPF2 + 0.75*CH$_2$O + HO$_2$
36	MT-bRO$_2$ \ MT-cRO$_2$ \ MT-HOM-RO$_2$ + CH$_3$O$_2$ → 0.15*CH$_3$OH + 0.85*CH$_2$O + 1.4*HO$_2$ + 0.7*HYDRALD + 0.7*CH$_3$COCH$_3$ + 0.15*C$_{10}$-ROH + 0.15*C$_{10}$-CBYL
37	MT-bRO$_2$ \ MT-cRO$_2$ \ MT-HOM-RO$_2$ + CH$_3$CO$_3$ → 0.7*CH$_3$O$_2$ + 0.7*HO$_2$ + 0.7*HYDRALD + 0.7*CH$_3$COCH$_3$ + 0.3*CH$_3$COOH + 0.15*C$_{10}$-ROH + 0.15*C$_{10}$-CBYL
38	APINO$_2$ + NO → 0.05*MT-bRO$_2$ + 0.0095*TERPHFN + 0.019*TERPNS1 + 0.095*TERPNS + 0.0475*TERPNT + 0.0475*TERPNT1 + 0.77*NO$_2$ + 0.77*HO$_2$ + 0.285*TERPA + 0.2565*TERPA3 + 0.09*CH$_3$COCH$_3$ + 0.0855*TERPF1 + 0.21*CH$_2$O + 0.1045*TERP1OOH
39	APINO$_2$ + NO$_3$ → 0.05*MT-bRO$_2$ + NO$_2$ + HO$_2$ + 0.3705*TERPA + 0.3325*TERPA3 + 0.12*CH$_3$COCH$_3$ + 0.114*TERPF1 + 0.27*CH$_2$O + 0.133*TERP1OOH
40	BPINO$_2$ + NO → 0.05*MT-bRO$_2$ + 0.08*CH$_3$COCH$_3$ + 0.49*CH$_2$O + 0.19*TERPF1 + 0.228*TERPK + 0.038*TERPNS1 + 0.019*TERPNS + 0.057*TERPNT + 0.1235*TERPNT1 + 0.2945*TERPA3 + 0.75*HO$_2$ + 0.75*NO$_2$
41	BPINO$_2$ + NO$_3$ → 0.05*MT-bRO$_2$ + 0.11*CH$_3$COCH$_3$ + 0.65*CH$_2$O + 0.2565*TERPF1 + 0.304*TERPK + 0.3895*TERPA3 + HO$_2$ + NO$_2$
42	LIMONO$_2$ + NO → 0.05*MT-bRO$_2$ + 0.1615*TERPNT1 + 0.057*TERPNS1 + 0.77*NO$_2$ + 0.7315*TERPF1 + 0.77*HO$_2$ + 0.43*CH$_2$O
43	LIMONO$_2$ + NO$_3$ → 0.05*MT-bRO$_2$ + NO$_2$ + 0.95*TERPF1 + HO$_2$ + 0.56*CH$_2$
44	MYRCO$_2$ + NO →

	0.05*MT-bRO$_2$ + 0.095*TERPNS1 + 0.1805*TERPNT1 + 0.71*NO$_2$ + 0.6745*TERPF2 + 0.33*CH$_3$COCH$_3$ + 0.3*CH$_2$O + 0.71*HO$_2$
45	MYRCO$_2$ + NO$_3$ → 0.05*MT-bRO$_2$ + NO$_2$ + 0.95*TERPF2 + 0.46*CH$_3$COCH$_3$ + 0.42*CH$_2$O + HO$_2$
46	MT-bRO$_2$\MT-cRO$_2$ + NO → 0.01*TERPHFN + 0.02*TERPNS1 + 0.1*TERPNS + 0.05*TERPNT + 0.05*TERPNT1 + 0.77*NO$_2$ + 0.77*HO$_2$ + 0.3*TERPA + 0.27*TERPA3 + 0.09*CH$_3$COCH$_3$ + 0.09*TERPF1 + 0.21*CH$_2$O + 0.11*TERP1OOH
47	MT-bRO$_2$+ NO$_3$ → HO$_2$ + NO$_2$ + 0.3*C$_{10}$-CBYL + 0.7*HYDRALD + 0.7*ROH
48	MT-cRO$_2$ + NO$_3$ → HO$_2$ + NO$_2$ + 0.75*C$_{10}$-CBYL + 0.25*MT-HOM-RO$_2$
49	MT-bRO$_2$\MT-cRO$_2$ + HO$_2$ → 0.06*CH$_3$COCH$_3$ + 0.06*TERPF1 + 0.08*CH$_2$O + 0.25*TERP1OOH + 0.48*HO$_2$ + 0.4*TERPOOH + 0.29*TERPA + 0.35*OH

4. Sink of newly added species

Reaction 50-52 show the chemical loss of three kinds of intermediate products (C10-CBYL, C10-ROH, and ROH) by reacting with OH radical (Table S4). All the newly added SOAG and SOA follows the same deposition processes with the original SOA and SOAG in VBS approach. Only particle-phase C$_{10}$ HOMs undergo photolysis process and the photolysis rate is set as about 1/60 of NO$_2$ photolysis rate (Xu et al., 2022).

Table S4. Chemical loss of C$_{10}$-CBYL and C$_{10}$-ROH

Index	Reactions
50	C$_{10}$-CBYL + OH → 0.125*APINO$_2$ + 0.125*BPINO$_2$ + 0.125*MYRCO$_2$ + 0.125*LIMONO$_2$ + 0.475*MT-bRO$_2$ + 0.025*MT-cRO$_2$
51	C$_{10}$-ROH + OH → 0.125*APINO$_2$ + 0.125*BPINO$_2$ + 0.125*MYRCO$_2$ + 0.125*LIMONO$_2$ + 0.475*MT-bRO$_2$ + 0.025*MT-cRO$_2$
52	ROH + OH → HO$_2$ + CH$_3$COCH$_3$

Table S5. Species for HOMs and ACC formation mechanism.

Species	Molecular formula	Description
APIN [b]	C$_{10}$H$_{16}$	α-pinene
BPIN [b]	C$_{10}$H$_{16}$	β-pinene
LIMON [b]	C$_{10}$H$_{16}$	Limonene
MYRC [b]	C$_{10}$H$_{16}$	Myrcene
APINO$_2$ [b]	C$_{10}$H$_{17}$O$_3$	peroxy radical from OH +α-pinene reaction

$BPINO_2$ [b]	$C_{10}H_{17}O_3$	peroxy radical from OH +β-pinene reaction
$LIMONO_2$ [b]	$C_{10}H_{17}O_3$	peroxy radical from OH + limonene
$MYRCO_2$ [b]	$C_{10}H_{17}O_3$	peroxy radical from OH + myrcene
$ISOPB1O_2$ [b]	$C_5H_9O_3$	OH-1-O_2-2—isoprene hydroxy peroxy radical
$ISOPZD1O_2$ [b]	$C_5H_9O_3$	OH-1-O_2-4-Z—isoprene hydroxy peroxy radical
$ISOPZD4O_2$ [b]	$C_5H_9O_3$	OH-4-O_2-1-Z—isoprene hydroxy peroxy radical
$ISOPED1O_2$ [b]	$C_5H_9O_3$	OH-1-O_2-4-E—isoprene hydroxy peroxy radical
$ISOPED4O_2$ [b]	$C_5H_9O_3$	OH-4-O_2-1-E—isoprene hydroxy peroxy radical
$ISOPB4O_2$ [b]	$C_5H_9O_3$	OH-4-O_2-3—isoprene hydroxy peroxy radical
MT-bRO_2 [a]	$C_{10}H_{16}O_4$	RO_2 from monoterpene+O_3/OH that can undergo autoxidation
MT-cRO_2 [a]	$C_{10}H_{16}O_6$	RO_2 from MT-bRO_2 autoxidation
MT-HOM-RO_2 [a]	$C_{10}H_{16}O_8$	RO_2 from MT-cRO_2 autoxidation
SOAGhma [a]	$C_{10}H_{14}O_9$	gas-phase C10 HOMs product without nitrate from HO_2 reaction
SOAGhmb [a]	$C_{10}H_{14}O_9$	gas-phase C10 HOMs product without nitrate from NO and NO_3 reaction
SOAGhmn [a]	$C_{10}H_{14}O_9N$	gas-phase C10 HOMs product with nitrate from NO reaction
SOAGac15 [a]	$C_{15}H_{18}O_7$	gas-phase C15 accretion product from isoprene-derived RO_2 (ISOP-RO_2) + MT-RO_2
SOAGac20 [a]	$C_{20}H_{32}O_8$	gas-phase C20 accretion product from MT-RO_2 + MT-RO_2
ROH [a]	C_3H_8O	lumped alcohols with more than 2 carbons
C_{10}-CBYL [a]	$C_{10}H_{17}O_3$	Carbonyl with 10 carbon atoms
C_{10}-ROH [a]	$C_{10}H_{17}O_3$	Alcohol with 10 carbon atoms
BIGALK	C_5H_{12}	lumped alkanes C>3
CH_2O [b]	CH_2O	formaldehyde
CH_3O_2 [b]	CH_3O_2	methylperoxy radical
CH_3CO_3 [b]	CH_3CO_3	acetylperoxy radical
CH_3COCH_3 [b]	CH_3COCH_3	acetone
CH_3COOH [b]	CH_3COOH	acetic acid
CH_3OH [b]	CH_3OH	methanol
HO_2 [b]	HO_2	hydroperoxyl radical
H_2O_2 [b]	H_2O_2	hydrogen peroxide
HCOOH [b]	HCOOH	formic acid
HMHP [b]	CH_4O_3	hydroxy methyl hydroperoxide
HYAC [b]	CH_3COCH_2OH	hydroxyacetone
HYDRALD [b]	$HOCH_2CCH_3CHCHO$	lumped unsaturated hydroxycarbonyl
TERP1OOH [b]	$C_{10}H_{18}O_3$	terpene-derived hydroxy hydroperoxide with 1 double bond
TERPA [b]	$C_{10}H_{16}O_2$	aldehyde terpene product with no double bonds that contains a ring like pinonaldehyde
TERPACID [b]	$C_{10}H_{16}O_4$	carboxylic acid/peracid from TERPA
TERPA2 [b]	$C_9H_{14}O_2$	TERPA oxidation product with no double bonds that contains an aldehydic group
$TERPA2O_2$ [b]	$C_9H_{15}O_4$	TERPA peroxy radical 2nd step
$TERPA2CO_3$ [b]	$C_9H_{13}O_4$	acyl peroxy radical from TERPA2
TERPA3 [b]	$C_9H_{14}O_3$	aldehyde terpene product with no ring like limonaldehyde
$TERPA3CO_3$ [b]	$C_9H_{13}O_5$	acyl peroxy radical from TERPA3
TERPF1 [b]	$C_{10}H_{16}O_2$	functionalized terpene product with 1 double bond typically containing carbonyl groups

TERPF2 [b]	$C7H_{10}O$	functionalized terpene product with 2 double bonds typically containing carbonyl groups
TERPHFN [b]	$C_{10}H_{19}NO_7$	terpene highly functionalized nitrate
TERPK [b]	$C_9H_{14}O$	terpene product containing a ketone group
TERPNS [b]	$C_{10}H_{17}NO_4$	terpene-derived saturated secondary or primary nitrate
TERPNS1 [b]	$C_{10}H_{17}NO_4$	terpene-derived unsaturated secondary or primary nitrate
TERPNT [b]	$C_{10}H_{17}NO_4$	terpene-derived saturated tertiary nitrate
TERPNT1 [b]	$C_{10}H_{17}NO_4$	terpene-derived unsaturated tertiary nitrate

[a] Xu et al. (2022)

[b] Schwantes et al. (2020)

We chose the main chemical reactions and descriptions and then added them into the **Supplement**:

"Figure S1 shows a flowchart of the HOMs mechanism implemented into CAM6-Chem and Table S1 shows the main chemical reactions added into CAM6-Chem. In general, monoterpenes (including α-pinene, β-pinene, limonene and myrcene) are oxidized by OH radicals or O_3 to form MT-aRO_2 and MT-bRO_2 radicals (reactions 1-2 listed in Table S1, with only reactions involving α-pinene shown as an example). MT-bRO_2 undergo multi-step autoxidation reactions to form HOMs with 10 carbon atoms (C10-HOMs) (green arrows in Fig. S1 and reactions 3-4 in Table S1). The intermediates for the autoxidation are MT-cRO_2 and MT-HOM-RO_2. The MT-HOM-RO_2 radical represents the RO_2 radicals that undergo two or multi-step autoxidation. On the one hand, MT-HOM-RO_2 radicals are further oxidized to form C10-HOMs (reaction 8-10 in Table S1). On the other hand, all the MT-RO_2 radicals (including MT-aRO_2, MT-bRO_2, MT-cRO_2, and MT-HOM-RO_2) undergo self- and cross-reactions (orange arrows in Fig. S1) to form accretion products (C15 and C20) (reactions 5-7 in Table S1, with only reactions involving MT-aRO_2 shown as an example). The formation processes of C10-HOMs can be terminated by several oxidants (gray arrows in Fig. S1). SOA is formed via gas-particle partitioning processes of C10-HOMs, C15 and C20 (blue dashed arrows in Fig. S1S1). "

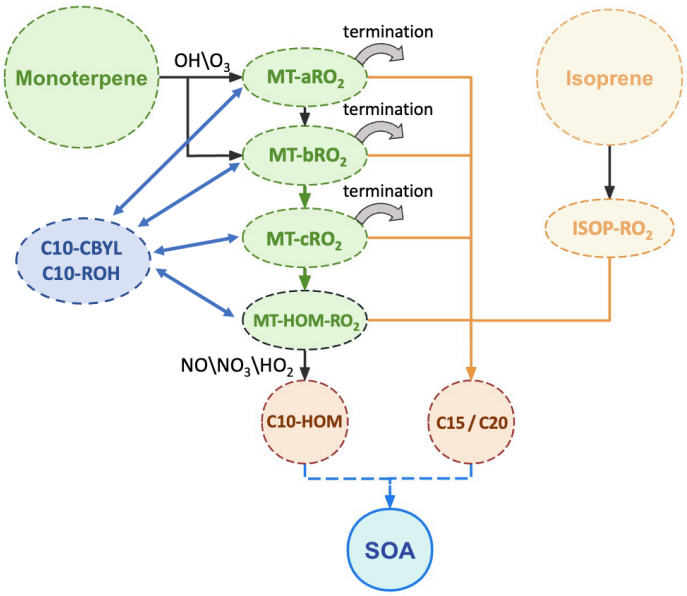

Figure S1. The flow chart of the formation and gas-particle partitioning processes of HOMs and accretion products. The green arrows represent the autoxidation reactions. The gray curved solid arrows represent the termination reactions. The yellow arrows represent the self- and cross-reactions. The blue arrows represent the conversion between C10-CBYL\C10-ROH and MT-RO_2 radicals. The blue dashed arrows represent the gas-particle partitioning processes.

Table S1. Main chemical reactions added in CAM6-Chem

Index	Reactions
1	APIN + OH → 0.25*$APINO_2$ + 0.75*MT-bRO_2
2	APIN + O_3 → 0.736*$APINO_2$ + 0.064*MT-bRO_2 + 0.77*OH + 0.066*$TERPA2O_2$ + 0.22*H_2O_2 + 0.044*TERPA + 0.002*TERPACID + 0.034*TERPA2 + 0.17*HO_2 + 0.17*CO + 0.27*CH_2O + 0.054*$TERPA2CO_3$
3	MT-bRO_2 → MT-cRO_2
4	MT-cRO_2 → MT-HOM-RO_2
5	MT-aRO_2 + MT-aRO_2 → 0.893*C_{10}-CBYL + 0.29*C_{10}-ROH + 0.603*HO_2 + 1.34*HYDRALD + 0.067*MT-bRO_2 + 0.04*SOAGac20
6	MT-aRO_2 + MT-bRO_2 → 0.96*C_{10}-CBYL + 0.29*C_{10}-ROH + 0.67*HO_2 + 1.34*HYDRALD + 0.04*SOAGac20
7	MT-aRO_2 + ISOP-RO_2 → 0.4465*C_{10}-CBYL + 0.145*C_{10}-ROH + 0.145*ROH + 0.603*HO_2 + 1.485*HYDRALD + 0.0335*MT-bRO_2 + 0.04*SOAGac15
8	MT-HOM-RO_2 + HO_2 → SOAGhma + O_2
9	MT-HOM-RO_2 + NO →

	$0.8*NO_2 + 0.8*HO_2 + 0.4*SOAGhmb + 0.8*HYDRALD + 0.2*SOAGhmn$
10	$MT\text{-}HOM\text{-}RO_2 + NO_3 \rightarrow$ $HO_2 + NO_2 + 0.5*SOAGhmb + HYDRALD$

Table S2. Species for HOMs and ACC formation mechanism.

Species	Molecular formula	Description
APIN [b]	$C_{10}H_{16}$	α-pinene
$APINO_2$ [b]	$C_{10}H_{17}O_3$	peroxy radical from OH +α-pinene reaction
$MT\text{-}bRO_2$ [a]	$C_{10}H_{16}O_4$	RO_2 from monoterpene+O_3/OH that can undergo autoxidation
$MT\text{-}cRO_2$ [a]	$C_{10}H_{16}O_6$	RO_2 from $MT\text{-}bRO_2$ autoxidation
$MT\text{-}HOM\text{-}RO_2$ [a]	$C_{10}H_{16}O_8$	RO_2 from $MT\text{-}cRO_2$ autoxidation
SOAGhma [a]	$C_{10}H_{14}O_9$	gas-phase C10 HOMs product without nitrate from HO_2 reaction
SOAGhmb [a]	$C_{10}H_{14}O_9$	gas-phase C10 HOMs product without nitrate from NO and NO_3 reaction
SOAGhmn [a]	$C_{10}H_{14}O_9N$	gas-phase C10 HOMs product with nitrate from NO reaction
SOAGac15 [a]	$C_{15}H_{18}O_7$	gas-phase C15 accretion product from isoprene-derived RO_2 ($ISOP\text{-}RO_2$) + $MT\text{-}RO_2$
SOAGac20 [a]	$C_{20}H_{32}O_8$	gas-phase C20 accretion product from $MT\text{-}RO_2$ + $MT\text{-}RO_2$
ROH [a]	C_3H_8O	lumped alcohols with more than 2 carbons
C_{10}-CBYL [a]	$C_{10}H_{17}O_3$	Carbonyl with 10 carbon atoms
C_{10}-ROH [a]	$C_{10}H_{17}O_3$	Alcohol with 10 carbon atoms
CH_2O [b]	CH_2O	formaldehyde
HO_2 [b]	HO_2	hydroperoxyl radical
H_2O_2 [b]	H_2O_2	hydrogen peroxide
HYDRALD [b]	$HOCH_2CCH_3CHCHO$	lumped unsaturated hydroxycarbonyl
TERPA [b]	$C_{10}H_{16}O_2$	aldehyde terpene product with no double bonds that contains a ring like pinonaldehyde
TERPACID [b]	$C_{10}H_{16}O_4$	carboxylic acid/peracid from TERPA
TERPA2 [b]	$C_9H_{14}O_2$	TERPA oxidation product with no double bonds that contains an aldehydic group
$TERPA2O_2$ [b]	$C_9H_{15}O_4$	TERPA peroxy radical 2nd step
$TERPA2CO_3$ [b]	$C_9H_{13}O_4$	acyl peroxy radical from TERPA2

Reference

Xu, R. C., Thornton, J. A., Lee, B., Zhang, Y. X., Jaegle, L., Lopez-Hilfiker, F. D., Rantala, P., and Petaja, T.: Global simulations of monoterpene-derived peroxy radical fates and the distributions of highly oxygenated organic molecules (HOMs) and accretion products, Atmos. Chem. Phys., 22, 5477-5494, 10.5194/acp-22-5477-2022, 2022.

Schwantes, R. H., Emmons, L. K., Orlando, J. J., Barth, M. C., Tyndall, G. S., Hall, S. R., Ullmann, K., St. Clair, J. M., Blake, D. R., Wisthaler, A., and Bui, T. P. V.: Comprehensive isoprene and

terpene gas-phase chemistry improves simulated surface ozone in the southeastern US, Atmos. Chem. Phys., 20, 3739-3776, 10.5194/acp-20-3739-2020, 2020.

Minor Comment#4: Table 1: Are these C* (300 K) values?

Response: Yes. Thanks for suggestions and we have added this information in Table 1.

Minor Comment#5: Eqn 7-8: Are all accretion products considered as part of [ACC]? Heinritzi et al (2020) showed that the formation of C15s from isoprene and monoterpene cross-reactions led to lower nucleation rates suggesting these do not participate in pure organic nucleation, (at least under (organic) supersaturation conditions in that work).

Response: Yes, in our simulation, all accretion products are considered as part of [ACC].

When simulating sub-20nm growth rate, we considered the suppression of C15 dimer. Similar to C20 dimer, the formation of C15 also consume the monoterpene derived RO_2 radicals (MT-RO_2), which in turn reduces C20 production. However, compared to C20, C15 dimer has higher volatility, making it less likely to reach saturation at the atmosphere and condense on the preexisting aerosols. Therefore, the formation of C15 could decline the growth rate compared to that of C20.

When simulating nucleation rate at ~ 1.7nm, we did not consider the suppression of C15 and assumed that C15 and C20 contribute equally to the nucleation rate. Heinritzi et al. (2020) showed that when isoprene is added at +25°C with a constant ratio of isoprene to monoterpene carbon (R = 2), there is a reduction in the growth-controlling nucleation rate by approximately a factor of 2. In our simulation, this has the greatest impact in the Amazon region, where the concentrations of C15 and C20 are both very high and ratio of isoprene to monoterpene is often significantly greater than 2. Therefore, the ion-induced pure nucleation rate is clearly overestimated in Amazon, which is also the reason why surface cloud condensation nuclei (CCN) are significantly overestimated. However, Heinritzi et al. (2020) did not provide a clear nucleation parameterization scheme for us to simulate the impact of C15 on ion-induced pure nucleation rate. If we simply remove C15 from the total ACC concentration involved in nucleation, it may lead to underestimation of nucleation rate. Therefore, we roughly combined C15 and C20 together to serve as the total ACC concentration involved in nucleation. We have added this analysis of the reason for overestimation of N_{20} and CCN in Amazon at L359:

"Since we did not consider the suppression of C15 generated from isoprene and monoterpene derived RO_2 (MT-RO_2) radicals cross-reactions on nucleation rates (Heinritzi et al., 2020), the ion-induced pure organic nucleation rate is overestimated in Amazon, and hence, cloud condensation nuclei (CCN) at surface level are overestimated in Inorg_Org."

Reference

Heinritzi, M., Dada, L., Simon, M., Stolzenburg, D., Wagner, A. C., Fischer, L., Ahonen, L. R., Amanatidis, S., Baalbaki, R., Baccarini, A., Bauer, P. S., Baumgartner, B., Bianchi, F., Brilke, S., Chen, D., Chiu, R., Dias, A., Dommen, J., Duplissy, J., Finkenzeller, H., Frege, C., Fuchs, C., Garmash, O., Gordon, H., Granzin, M., El Haddad, I., He, X., Helm, J., Hofbauer, V., Hoyle, C. R., Kangasluoma, J., Keber, T., Kim, C., Kürten, A., Lamkaddam, H., Laurila, T. M., Lampilahti, J., Lee, C. P., Lehtipalo, K., Leiminger, M., Mai, H., Makhmutov, V., Manninen, H. E., Marten, R., Mathot, S., Mauldin, R. L., Mentler, B., Molteni, U., Müller, T., Nie, W., Nieminen, T., Onnela, A., Partoll, E., Passananti, M., Petäjä, T., Pfeifer, J., Pospisilova, V., Quéléver, L. L. J., Rissanen, M. P., Rose, C., Schobesberger, S., Scholz, W., Scholze, K., Sipilä, M., Steiner, G., Stozhkov, Y., Tauber, C., Tham, Y. J., Vazquez-Pufleau, M., Virtanen, A., Vogel, A. L., Volkamer, R., Wagner, R., Wang, M., Weitz, L., Wimmer, D., Xiao, M., Yan, C., Ye, P., Zha, Q., Zhou, X., Amorim, A., Baltensperger, U., Hansel, A., Kulmala, M., Tomé, A., Winkler, P. M., Worsnop, D. R., Donahue, N. M., Kirkby, J., and Curtius, J.: Molecular understanding of the suppression of new-particle formation by isoprene, Atmos. Chem. Phys., 20, 11809-11821, 10.5194/acp-20-11809-2020, 2020.

Minor Comment#6: Paragraph at line 260: Can this analysis be made clearer? Why does an overestimation of H_2SO_4 lead to and underestimation in growth rate overall, but then also explains overestimated growth rates in specific cities?

Response: Response: We apologize for the unclear description. We have added the explanation at line 261:

"The underestimation of the sub-20nm growth rate in Inorg is due to an almost zero nucleation rate at around 1nm. Consequently, the absence of a nucleation rate results in the absence of NPF events and, thus, a zero growth rate. In contrast, in Inorg_Org, the NPF frequency is simulated accurately compared to that in Inorg (Fig, 1c). One contributing factor to the overestimation of the growth rate in Inorg_Org is the overestimation of the H_2SO_4 concentration, a feature of CAM6, as evidenced by comparisons with previous model simulations (Table S5) and measurements (Table S6)."

Minor Comment#7: Over- or underestimations in condensation sink are occasionally used to justify a corresponding under- or overestimation in NPF. This makes sense, however, can CS be prescribed in order to validate this?

Response: We are unable to implement this because the condensation sink (CS) is calculated online in the model. If we were to use a prescribed value, it would require data to be input every half hour (as the physical timestep of CAM6-Chem is half an hour). However, CS derived from measurements cannot provide such high temporal precision.

Minor Comment#8: Figure 4c, d can a label and the units be places under the x-axis?

Response: Thanks for reminding. We added the unit of N_{20} and CCN (cm^{-3}) under the x-axis. The new figure is shown as follow.

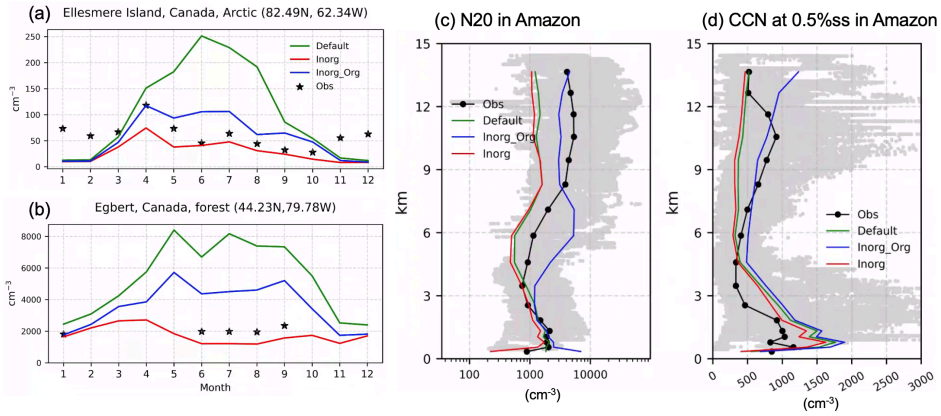

Minor Comment#9: Line 340: Is the "organic nucleation rate" mentioned here just the sum of the neutral ($J_{Org,n}$) and ion-induced pure organic nucleation ($J_{Org,i}$) or does it also include inorganic-organic nucleation ($J_{SA\text{-}Org}$)?

Response: Yes. We apologize for the missing information in that sentence. The We have modified the sentence as follows.

"Globally, the vertically-integrated (below 15 km) annual mean organic nucleation rate ($J_{Org,n}$+$J_{Org,i}$+J_{SA-Org}) in Inorg_Org is 32 ×10^6 cm^{-2} s^{-1} (Fig. 5a), closely matching the inorganic nucleation rate of 39 ×10^6 cm^{-2} s^{-1} (Table 4)."

Minor Comment#10 and # 11: Figure 9: There are 2 panels labeled g.

Figure 9: There is only 1 unit given in the caption, but the left and right plots appear to have different units.

Response: We apologize for the spelling error and missing information in Figure 9. The new version of Figure 9 is as follow:

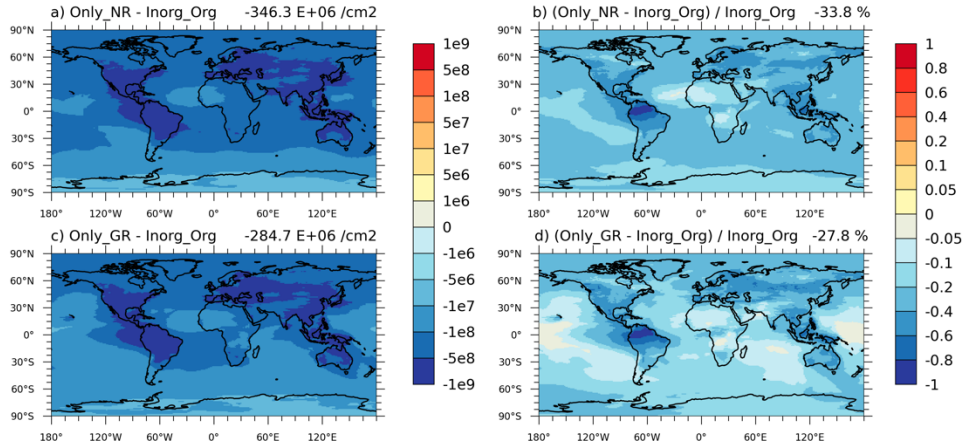

Figure 9: Absolute differences (Units: cm^{-2}) and relative differences (Units: unitless) of in total vertically-integrated aerosol numbers in July 2013 between Inorg_Org and other sensitivity tests. Global mean values are shown on the top right of each figure. Model experiments are described in Table 2.

We have added a new **Section 5** to analyze the impact of uncertainties from HOMs chemistry on aerosol and CCN numbers. Consequently, the discussions regarding the differences from Low_Br, as well as Slow_NO and Inorg_Org, have been moved to Section 5.

Minor Comment#12: Figure 10: There is reference in the caption to up to panel h, but the figure only contains up to panel d.

Response: We apologize for the wrong information in the caption and have corrected this. Now Figure 10 is as follow:

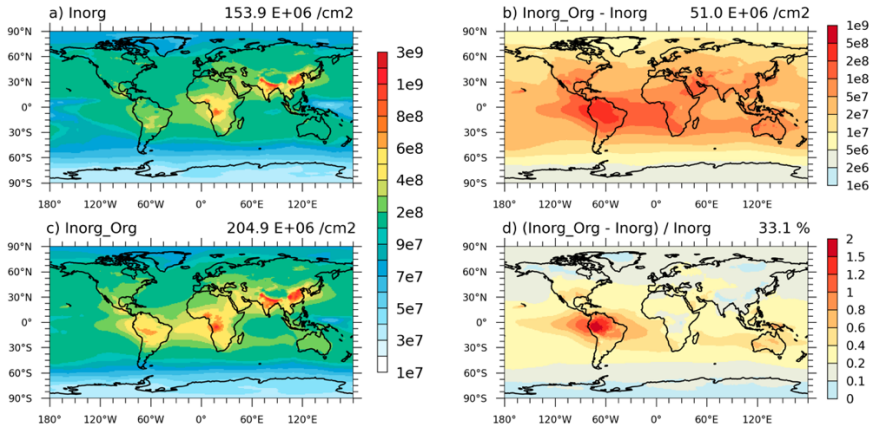

Figure 10: Spatial distribution of annual mean total vertically-integrated CCN concentrations at 0.5% supersaturation for (a) Inorg and (c) Inorg_Org (unit: cm^{-2}). Also, (b) change and (d) relative change are shown. Global mean values are shown on the top right of each figure.